

# Phylogeny of *Weinmannia* (Cunoniaceae) reveals the Contribution of the Southern Extratropics to Tropical Andean Biodiversity.

Ricardo A. Segovia\*<sup>1,2</sup>, Eduardo Aguirre-Mazzi\*<sup>3,4</sup>, Christine E. Edwards<sup>5</sup>, Alexander G. Linan<sup>6</sup>, Alfredo Fuentes<sup>4,7</sup>, Andrea Chaspuengal<sup>8</sup>, Kyle G. Dexter<sup>9,10</sup>, Francisco Fajardo<sup>11</sup>, William Farfan-Rios<sup>12,13</sup>, Nora H. Oleas<sup>8</sup>, Juan C. Penagos Zuluaga<sup>14</sup>, J. Sebastián Tello<sup>4</sup>

## Abstract

The Andes are a relatively young mountain range with impressive biodiversity, but the biogeographic processes underlying its hyperdiversity are still being unraveled. Novel mid- to high-elevation climates may have served as a biological corridor for the immigration of temperate-adapted lineages to lower latitudes, contributing unknown levels of diversity to this region. We tested the hypothesis that *Weinmannia* is a lineage of extratropical origin that recently reached and then diversified extensively in tropical Andes. Using a 2bRAD seq approach to generate a time-calibrated phylogeny for the genus, we found that extratropical species were placed as sister to the rest of *Weinmannia* and that younger clades were distributed towards northern latitudes. Although *Weinmannia* exhibited low niche conservatism in elevation and latitude, trait reconstructions of mean annual temperature showed that the common ancestor of *Weinmannia* occupied cool climates, with high conservatism of thermal niche across the phylogeny. Thus, Andean uplift likely created habitats with suitable temperatures, providing a dispersal route for *Weinmannia* to colonize the tropical Andes from the southern extratropics. These southern lineages likely converged with those originating in other tropical and extratropical centers of diversification, providing multiple origins for the hyperdiversity in the modern montane forests of the tropical Andes.

**Keywords:** immigration, diversification, hyperdiversity, tropics, Gondwana

<sup>1</sup>Departamento de Botánica, Universidad de Concepción, Chile; <sup>2</sup>Institute of Ecology and Biodiversity (ieb-chile.cl); <sup>3</sup>Department of Biology, Washington University in St. Louis, St. Louis, MO, United States; <sup>4</sup>Latin America Department, Missouri Botanical Garden, St. Louis, MO, United States; <sup>5</sup>Center for Conservation and Sustainable Development, Missouri Botanical Garden, St. Louis, MO, United States; <sup>6</sup>Africa and Madagascar Program, Missouri Botanical Garden, St. Louis, MO, United States; <sup>7</sup>Herbario Nacional de Bolivia, Instituto de Ecología, Carrera de Biología, Universidad Mayor de San Andrés, La Paz, Bolivia.; <sup>8</sup>Centro de Investigación de la Biodiversidad y Cambio Climático (BioCamb) y Facultad de Ciencias del Medio Ambiente, Universidad Tecnológica Indoamérica, Machala y Sabanilla, Quito, Ecuador; <sup>9</sup>School of GeoSciences, University of Edinburgh; <sup>10</sup>Royal Botanic Garden Edinburgh; <sup>11</sup>14195 Berlin, Germany; <sup>12</sup>Department of Biology, Wake Forest University, Winston-Salem, NC 27106, USA.; <sup>13</sup>Andrew Sabin Center for Environment and Sustainability, Wake Forest University, Winston-Salem, NC 27106, USA.; <sup>14</sup>Research Affiliate Yale School of the Environment, Yale University, 195 Prospect Street, New Haven, CT.; \* These authors contributed equally to this work

Corresponding author; e-mail:

rsegovia@ieb-chile.cl;  
christine.edwards@mobot.org

## 1. Introduction

The Andean region of tropical America has one of the world's highest levels of species richness (Balslev, 1993), taxonomic endemism (Myers et al., 2000) and phylogenetic diversity (Tietje et al., 2023). This hyperdiversity is particularly intriguing given that the modern geomorphology of this area is no older than the late Miocene (< 11 Ma) (Gregory-Wodzicki, 2000; Siravo et al., 2018). Mountain building is generally thought to have fostered high diversity both through speciation of resident lineages (Rahbek et al., 2019) and the immigration of lineages pre-adapted to newly created climatic conditions (Donoghue, 2008). Indeed, the Andean orogeny may have increased the rate of lineage diversification (Antonelli and Sanmartin, 2011a) and may also have opened a corridor for the immigration of temperate lineages into the lower latitudes of tropical America (Graham, 1973, Segovia and Armesto, 2015). Comprehensive evolutionary evidence is still being gathered to identify areas of lineage origin and thus unravel the relative influence of these biogeographic processes in shaping the modern pattern of hyperdiversity in the Andes.

Phylogenetic evidence shows faster-than-expected rates of diversification for a number of potentially resident plant clades in synchrony with the Andean uplift since the early Miocene (e.g.,

Luebert and Weigend, 2014; Pérez-Escobar et al., 2022). Moreover, 23  
a growing body of phylogenetic evidence shows immigration from 24  
both the northern and southern extratropics into the tropical Andes. 25  
Many lineages have immigrated from the northern extratropics, 26  
including *Viburnum* (Winkworth and Donoghue, 2005), *Lupinus* 27  
(Hughes and Eastwood, 2006), and *Passiflora* section *Decaloba* 28  
(Acha et al., 2021). Conversely, there is less evidence of lineages 29  
immigrating from the southern extratropics to the tropical Andes, 30  
although notable examples include Alstroemeriaceae (Chacón et 31  
al., 2012), *Podocarpus* (Quiroga et al, 2016), *Gunnera* (Bacon et 32  
al., 2018), and Loranthaceae (Liu et al., 2018). However, most of 33  
what we know about these biogeographic scenarios for the origin of 34  
the plant diversity in the tropical Andes has disproportionately 35  
focused on taxa inhabiting open biomes at high-elevations. 36  
Evidence regarding the origin and direction of dispersal routes of 37  
the clades that occupy montane forests at intermediate elevations 38  
remains scarce, representing a significant gap in our understanding 39  
of plant diversity and evolution in one the most species-rich regions 40  
on the planet. 41

The idea that lineages from the relatively species-poor 42  
extratropics could contribute to the modern hyperdiversity of the 43  
tropical Andes is counterintuitive. Traditionally, the highest levels 44

of species richness are thought to be associated with "centers of 45  
diversification" (Willis, 1922), or areas where a particular lineage 46  
originated (Wiens and Donoghue, 2004), and there is strong 47  
evidence that the American tropics have historically acted as a 48  
"species pump" for global plant diversity (Antonelli et al., 2015). 49  
However, immigration from multiple zones, including the 50  
extratropics, into tropical Andean forests has been identified based 51  
on taxonomic affinities (Hooghiemstra, 1984), fossil records 52  
(Graham, 1995), and community phylogenetics (González-Caro et 53  
al., 2023), not just through clade reconstructions. These multi- 54  
source immigration processes, along with rapid lineage 55  
diversification, may be key to shaping the modern hyperdiversity of 56  
the tropical Andes, increasing not only taxonomic diversity but also 57  
evolutionary diversity, according to the "environmental crossroads 58  
hypothesis" (Neves et al., 2020). For example, the exceptionally 59  
high phylogenetic diversity found in the central and northern Andes 60  
(Tietje et al., 2023) may be due to the mixing of deeply isolated 61  
biotas with different evolutionary histories (e.g., remnants of 62  
paleobiotas from the Holarctic, Austral and Neotropical floristic 63  
realms). 64

Here we investigate the biogeography of *Weinmannia* L. 65  
(*sensu* Pillon et al., 2021), formerly *Weinmannia* sect. *Weinmannia* 66

L. (Bradford, 1998), an important genus of trees and shrubs at 67  
Andean forests, given their high abundance and diversity. Typically 68  
considered an extratropical southern hemisphere taxon (Raven and 69  
Axelrod, 1974), *Weinmannia* comprises two species occurring in 70  
the Mascarenes and over 80 species in the Americas (Bradford, 71  
1998, 2002, Pillon et al., 2021). Most *Weinmannia* species occur at 72  
mid- to high- elevations in the tropical Andes, where they exhibit 73  
weak species boundaries and overlapping morphologies due to 74  
either recent divergence or hybridization (Bradford, 1998, 2002). In 75  
addition, several species occur in the Guiana shield and mountain 76  
peaks of Central America and the Caribbean Islands. One species is 77  
endemic to the subtropical forests of eastern Brazil (i.e., Mata 78  
Atlantica), and another occurs in the temperate forests of southern 79  
South America (Chile and Argentina). Previous phylogenies placed 80  
the only southern extratropical species (*Weinmannia trichosperma* 81  
Cav.) as an early diverging lineage of *Weinmannia* (Bradford, 82  
1998, 2002), sparking the hypothesis that *Weinmannia* immigrated 83  
recently into the tropical Andes from the southern extratropics 84  
(Bradford et al., 2004; Pennington and Dick, 2004). However, these 85  
analyses sampled only a small proportion of the species in the 86  
genus and employed only a small number of plastid and/or nuclear 87  
regions (Bradford, 2002; Pillon et al., 2021), preventing hypothesis 88

testing about the origin and dispersal of <i>Weinmannia</i> across the	89
Andes.	90
To examine the hypothesis of a southern extratropical origin	91
for <i>Weinmannia</i> and its recent immigration into the tropical Andes,	92
we reconstructed a new NGS phylogeny with dense taxon	93
sampling. First, we tested the prediction that if the genus	94
<i>Weinmannia</i> originated in the southern extratropics, then <i>W.</i>	95
<i>trichosperma</i> from the temperate forests of southern South America	96
and other southern lineages should be resolved as the sister lineages	97
to all other American <i>Weinmannia</i> species and should have	98
originated in a node closer to the root, reflecting their ancestral	99
status within the genus. Second, we tested the prediction that if the	100
modern distribution of <i>Weinmannia</i> in the Americas is a	101
consequence of dispersal from the southern extratropics into the	102
tropical Andes, then the ages of nodes in the phylogeny should	103
show a negative relationship with the reconstructed latitude of the	104
nodes. In other words, the phylogeny should show a pattern in	105
which younger clades occupy successively more northern latitudes.	106
Additionally, we explored whether the evolution of the thermal	107
niche of <i>Weinmannia</i> reflects phylogenetic conservatism of	108
lineages originating from extratropical climates.	109
	110

<b>2. Materials &amp; Methods</b>	111
<b>2.1. Sampling and genomic DNA extraction.</b> We collected 896	112
samples of <i>Weinmannia</i> from across South America, including the	113
southern Andes (Chile), the central Andes (Bolivia and Peru), and	114
the northern Andes (Ecuador and Colombia). We also included four	115
samples from the Mascarene Islands. For each sample, we	116
preserved leaf tissue in silica and collected an herbarium voucher	117
specimen. In addition, we included five specimens from three	118
species of <i>Pterophylla</i> ( <i>sensu</i> Pillon et al., 2021) as outgroups.	119
To extract DNA, silica-dried tissues were ground and	120
cleaned using up to three sorbitol washes following Inglis et al.	121
(2018) to remove mucilage and other secondary compounds.	122
Genomic DNA was extracted using a modified CTAB extraction	123
protocol for plants (based on Doyle and Doyle 1987), with	124
additional ethanol washes of precipitated DNA. Following	125
extraction, DNA was purified using KAPA pure Beads (KAPA	126
Biosystems) following manufacturer protocols. DNA	127
concentrations were quantified using a Qubit™ fluorometer	128
(ThermoFisher).	129
<b>2.2. Sequencing.</b> RAD-seq libraries were prepared using a 2b-	130
RAD approach (Wang et al., 2012) following previously published	131

protocols (Linan et al., 2021b; Mashburn et al., 2023). We digested	132
500 ng of purified genomic DNA of each sample using the BcgI	133
restriction enzyme (New England Biolabs), producing 36 bp DNA	134
fragments from across the genome. To ensure adequate sequence	135
coverage per locus, 5'-NNG-3' selective adapters were used	136
decreasing the number of sequenced loci (Wang et al., 2012). 96	137
samples were pooled per plate using dual indexing, whereby the	138
first index was applied across columns, allowing pooling of the 8	139
rows. Each of these pools was amplified for 14 cycles of PCR	140
while incorporating the second index (one of eight unique 6 bp	141
Illumina TruSeq barcodes) using high-fidelity Phusion PCR mix	142
(New England Biolabs). The amplicons were visualized using 2%	143
Agarose gel electrophoresis and purified using the MinElute gel	144
purification kit (Qiagen). The purified ligation pools were	145
quantified using a Qubit fluorometer, pooled in equimolar	146
proportions (Qiagen), and sequenced on an Illumina HiSeq 4000,	147
generating 50 bp single end reads at the NUSeq Core facility of	148
Northwestern University.	149
<b>2.3. RAD locus assembly.</b> Sequences were demultiplexed and	150
trimmed to remove row and column indexes using the	151
trim2bRAD_2barcodes.pl script	152
( <a href="https://github.com/z0on/2bRAD_denovo">https://github.com/z0on/2bRAD_denovo</a> ). Trimmed reads were	153



assembled *de novo* in the ipyrad v. 0.9.90 pipeline (Eaton and Overcast, 2020). To determine the optimum clustering threshold, we iterated clustering threshold within samples (CTWS) and among samples (CTAS) using every combination of values of 0.86, 0.89, 0.92, and 0.94. The resulting matrices were compared for cluster depth, heterozygosity, the amount of putatively paralogous loci, and the number of SNPs to identify parameters that could lead to assembly errors (Paris et al., 2017). We selected a value of 0.92 for both CTWS and CTAS. All loci showing gaps or that had more than five SNPs were removed.

**2.4. Identification of putative hybrids.** To identify putative hybrid individuals that may confound phylogenetic analysis, we assessed admixture using STRUCTURE v. 2.3.4 (Pritchard et al., 2000) as implemented in ipyrad v. 0.9.90. Due to the large number of samples and putative species, we divided samples into two geographically structured datasets (central Andes region and northern Andes region), given that interspecific gene flow is most likely to occur among geographically proximal species. For each of these datasets we conducted an independent assembly, removing all individuals with more than 80% missing sites, retaining loci present in at least 50% of samples, and retaining one SNP per locus. STRUCTURE analyses were run testing values of  $K=2-20$  with a

burn-in of 300,000 generations, a run length of 700,000 176  
generations, and 15 replicates of each *K* value. The optimal *K* value 177  
was selected using the Evanno method (Earl and von Holdt, 2012). 178  
We defined putative hybrids as individuals with <85% assignment 179  
to a single genetic cluster, adopting a more conservative criterion 180  
compared to the 80% cut-off used by Owusu et al. (2015) and 181  
Linan et al. (2021b). 182

**2.5. Individual-level tree inference.** For phylogenetic inference, 183  
we chose 3–5 individuals with no signature of hybridization from 184  
each species, resulting in 234 accessions from 48 *Weinmannia* taxa 185  
(including 6 that are not assigned to any described species), plus 3 186  
*Pterophylla* species as outgroups (total=51 species). This dataset is 187  
a representative sample of the 75–90 estimated *Weinmannia* 188  
species occurring in the Americas (Pillon et al., 2021). 189

Maximum likelihood (ML) phylogenetic analysis was 190  
conducted using a concatenated dataset of the 36 bp loci, including 191  
invariant characters. First, we performed preliminary analysis to 192  
explore the effect of missing data on the resulting topologies, 193  
varying the percentage of samples at which a locus must be present 194  
from 4%–48% in increments of 4. We found optimal branching 195  
resolution and bootstrap support when all loci were present in at 196  
least 36% (84/234) of samples, which was used in the final 197

analysis. The ML phylogeny was inferred in RAxML v. 8.2.12 198  
(Stamatakis, 2014) using a rapid hill climbing algorithm and the 199  
GTRCAT approximation. Clade support was calculated using the 200  
transfer bootstrap approach with 200 iterations (Lemoine et al. 201  
2018). 202

**2.6. Species-level *Weinmannia* phylogeny.** To reconstruct a 203  
species-level phylogeny, we selected one representative individual 204  
from each species (*i.e.*, a reciprocally monophyletic group of 205  
individuals that had morphological distinctiveness) in the 206  
individual-level phylogeny (Supplementary Fig. 1). We chose the 207  
non-admixed individual (as indicated by STRUCTURE) with the 208  
least missing data. For phylogeny reconstruction, we employed 209  
both a ML analysis of the concatenated loci and SVDQuartets, 210  
which is a multi-species coalescent-based approach (Chifman and 211  
Kubatko, 2014). The species-level ML analysis used the same 212  
settings as described for the individual-level phylogeny. After 213  
preliminary analysis to explore the effect of missing data, we 214  
prepared a concatenated alignment of all loci present in at least 215  
32% (16/51) of all individuals, which was used to infer a 216  
phylogeny in RAxML. The multi-species coalescent-based 217  
phylogenetic inference was performed using a randomly selected 218  
SNP from each of the 2,879 loci used in the RAxML analysis. We 219

inferred all 249,900 possible quartets for 51 taxa and conducted 220  
500 bootstrap iterations. The quartet trees were joined into a super 221  
tree. Branch lengths for this topology were estimated in RAxML 222  
using the same alignment as in the ML phylogeny, with the -g 223  
option to constrain the topology. Finally, we calculated bootstrap 224  
support (BS) for nodes using a transfer bootstrap approach 225  
(Lemoine et al., 2018). For visualization, the resulting trees were 226  
rooted on the branch containing all *Pterophylla* specimens. 227

**2.7. Time-calibrated phylogeny.** We inferred node ages for both 228  
our ML and SVDQ trees using treePL (Smith and O'Meara, 2012), 229  
which relies on branch length information to estimate divergence 230  
times under phylogenetically penalized likelihood, following 231  
Maurin (2008). Optimal parameters for treePL were determined 232  
using the prime option, with the smoothing parameter estimated via 233  
cross-validation. Divergence time confidence intervals were 234  
calculated through a bootstrap analysis in RAxML, constraining 235  
topology with the ML tree (-g) and optimizing branch lengths (-k) 236  
over 200 bootstrap iterations. These bootstrap trees were time- 237  
calibrated using the same treePL parameters as the ML tree. A 238  
consensus tree was generated in TreeAnnotator v.2.5.2 (Drummond 239  
and Rambaut, 2007) using the estimated and bootstrap trees, with 240  
0% burn-in and median heights. 241

Three calibration points were defined for divergence time estimation. The first was a *Weinmannia* pollen fossil collected from the northern Andes of Colombia dated to ~3 million years ago (Ma) (Van Der Hammen et al., 1973). This age was defined as the minimum age for the most recent common ancestor of the clade that encompassed all specimens collected in the Northern Andes. The second point was derived from a fossil pollen record of *Weinmannia potosina* from Potosí, Bolivia from 13.8 Ma (Berry, 1917; Graham et al., 2001), which was established as the minimum age for the most recent common ancestor (MRCA) of the clade containing all Central and Northern Andean *Weinmannia* species. The upper limit for this point was set at 33 Ma, aligning with the proposed beginning of the Oligocene and previous estimates for the stem node of *Weinmannia* at 32.3 Ma (Pillon et al., 2021). Additionally, we used the 95% credibility interval with a minimum age of 29.99 Ma and a maximum age of 34.4 Ma, with a uniform distribution from Pillon et al. 2021, to estimate the divergence time between *Weinmannia* and its sister genus *Pterophylla*.

**2.8. Testing of our biogeographic hypotheses.** To test our hypothesis that *Weinmannia* migrated from south to north, we performed an ancestral reconstruction of latitude using our time-calibrated species-level phylogeny. We determined the minimum

and mean latitude for each species in the phylogeny based on geo- 264  
referenced occurrence data from herbarium specimens. Ancestral 265  
character estimation was conducted using the ‘anc.ML’ function in 266  
the phytools v. 2.1 R package (Revell, 2012). We compared the fit 267  
of the Brownian motion and Ornstein-Uhlenbeck models with the 268  
Akaike Information Criterion (AIC) (data not shown), selecting the 269  
Brownian motion for all subsequent analyses due to its better fit to 270  
the data. Ancestral reconstruction of both minimum and mean 271  
latitude was performed on a pruned phylogeny without outgroups. 272  
For hypothesis testing, we performed the analysis both with and 273  
without the two Mascarene species to assess the effect of these taxa 274  
(with the pruned dataset including a total of 46 South American 275  
species). We report only the minimum latitude results here, as the 276  
mean latitude estimates were equivalent but less reliable due to 277  
insufficient records for some species. Node ages were extracted 278  
from the time-calibrated phylogeny using the 279  
‘node.depth.edgelenh’ function in the ape v. 5.0 R package 280  
(Paradis and Schliep, 2019). Using data from the ancestral 281  
reconstruction, we modeled the age of hypothetical ancestors 282  
(nodes) as a function of their estimated latitudes using two distinct 283  
statistical approaches: a Bayesian approach and a frequentist 284

approach based on a Null-Hypothesis Significance Test and non- 285  
parametric bootstrapping. 286

**2.9. Bayesian regression analysis.** We developed a hierarchical 287  
Bayesian linear regression to assess correlation structures from 288  
nesting patterns between phylogenetic nodes, considering 289  
evolutionary relationships in latitude observations. The Bayesian 290  
regression tested the hypothesis that older ancestors are linked to 291  
more southern latitudes (*i.e.*, more negative values) leading to a 292  
negative slope (*i.e.*,  $\beta < 0$  to reject the null hypothesis of  $\beta \approx 0$ , 293  
implying no clear relationship). The model was fitted using four 294  
independent MCMC chains, each running 3,000,000 iterations. For 295  
efficiency, chains were thinned every 10 iterations, yielding 296  
300,000 samples per chain, with the first 50,000 discarded as burn- 297  
in. The max\_tree depth was set to 10 to address divergent 298  
transitions during sampling. We assessed model adequacy with a 299  
posterior predictive check, comparing predicted node ages to 300  
observed data (Fig. 3B, Supplementary Fig. 5B). MCMC 301  
performance was evaluated using Gelman-Rubin statistics (Rhat), 302  
effective sample size, and autocorrelation analysis (Supplementary 303  
Materials 2 and 3). We extracted the posterior probability 304  
distribution of the slope parameter ( $\beta$ ), along with 95% and 99% 305  
credibility intervals, and determined the maximum *a posteriori* 306

estimate. The model code, implemented in Stan v. 2.18.2	307
(Carpenter et al., 2017) and executed in R using the rstan package	308
v. 2.26.23 (Stan Development Team 2023), is provided in	309
Supplementary Materials and detailed explanation of model	310
equations and parameters is provided in Supplementary Materials	311
1.	312
<b>2.10. Non-parametric bootstrap Null Hypothesis Significance</b>	313
<b>Test (NHST).</b> As an alternative approach, we used the glm function	314
from the R package stats v. 3.6.2 (R Core Team 2023) to model node age	315
as a function of reconstructed ancestral latitude under a linear regression	316
framework. To find the model with the highest adequacy and fit, we	317
tested combinations of two probability distributions (Gaussian and	318
Gamma) and three link functions (identity, log and inverse) and	319
selected the model with the lowest AIC value, highest linearity of	320
predicted vs observed values (using qqplots) and better	321
homoscedasticity. For both the ML tree and SVDQ tree-based	322
analyses we selected gamma-distributed error and the identity	323
function (Supplementary Figures 6). We performed a bootstrap	324
analysis within the NHST framework with 10,000 iterations. In	325
each iteration, we randomized reconstructed node latitudes and	326
conducted regressions to obtain the slope parameter ( $\beta$ ). This	327
generated a null distribution for the slope. Because the observed	328



slope was negative, we calculated the p-value as the proportion of 329  
the null distribution less than or equal to the observed slope. 330

**2.11. Exploratory analysis of thermal niche conservatism.** To 331  
test the hypothesis that *Weinmannia* had an extratropical origin and 332  
migrated from south-to-north as uplift created a corridor of suitable 333  
habitats, we assessed thermal niche conservatism across the 334  
phylogeny. We performed ancestral reconstructions of mean annual 335  
temperature (BIO1) and elevation using our time-calibrated ML 336  
species-level phylogeny. BIO1 values were extracted from 337  
WorldClim 2 (Fick and Hijmans, 2017) at 0.5 arc-second 338  
resolution, and elevations were estimated from geo-referenced 339  
herbarium specimen data. To evaluate trait conservatism, we used a 340  
color gradient to map observed and reconstructed values onto the 341  
species-tree edges with the 'contMap' function in phytools v.2.1, 342  
under a Brownian motion model. Using reconstructed values of 343  
BIO1, Elevation, and Latitude, we calculated the darwin (d) rate of 344  
trait evolution per unit of time (Haldane 1949) for each node in the 345  
ML species-phylogeny, determining the relative change from the 346  
root node (putative extratropical ancestor) to each node. This 347  
allowed us to evaluate whether ancestral values at basal nodes were 348  
retained throughout the tree. We called this statistic  $d_{root}$ . To 349  
statistically assess differences in mean  $d_{root}$  between the 350

reconstructed traits, we employed a likelihood based framework 351  
based on generalized linear model (GLM) without an intercept to 352  
estimate the mean  $d_{root}$  for each trait. This model was compared 353  
through a likelihood ratio test assuming no difference between 354  
traits. Mean estimates not significantly different from zero 355  
indicated conservatism of ancestral traits throughout phylogeny. 356  
Pairwise t-tests were conducted to compare  $d_{root}$  means between 357  
traits. Finally, for each trait we performed a simple linear 358  
regression to evaluate if  $d_{root}$  varied across phylogenetic scales 359  
using wald-tests on slope parameters; slope values  $\approx 0$  suggest no 360  
shifts in  $d_{root}$  across phylogenetic scales whereas positive values 361  
would suggest higher changes in deeper nodes. A detailed 362  
explanation of these methods can be found in the Supplementary 363  
Methods. 364

### 3. Results 365

**3.1. Specimen-level phylogeny.** After identification and removal 366  
of putative hybrids, we obtained a dataset of 234 accessions for the 367  
specimen-level phylogeny (Fig. 1A, Supplementary Fig. 1, 368  
Supplementary Table 2). The concatenated alignment was 27,072 369  
bp in length (752 loci) and contained 31.91% missing data. In the 370  
371

ML phylogeny, all accessions of a given species formed 372  
monophyletic groups except for *Weinmannia reticulata* Ruiz & 373  
Pav. Two different subclades, named *W. reticulata1* and *W.* 374  
*reticulata2*, were treated as separate species for the purpose of the 375  
present analysis (Supplementary Fig. 1). Our analysis also included 376  
accessions of undetermined species (sp1–6) that showed 377  
morphological and phylogenetic cohesion. Overall, the specimen- 378  
level phylogeny showed strong geographic structure within South 379  
American *Weinmannia*, with clades each containing specimens 380  
collected in the same region. Species from the Northern Andes 381  
(Ecuador and Colombia) formed a clade nested within the 382  
*Weinmannia* crown group that included the species sampled from 383  
the Central Andes (Bolivia and Peru), Southern Andes (Chile) and 384  
Reunion Island (Fig. 1A, Supplementary Figs. 1,2). 385  
386

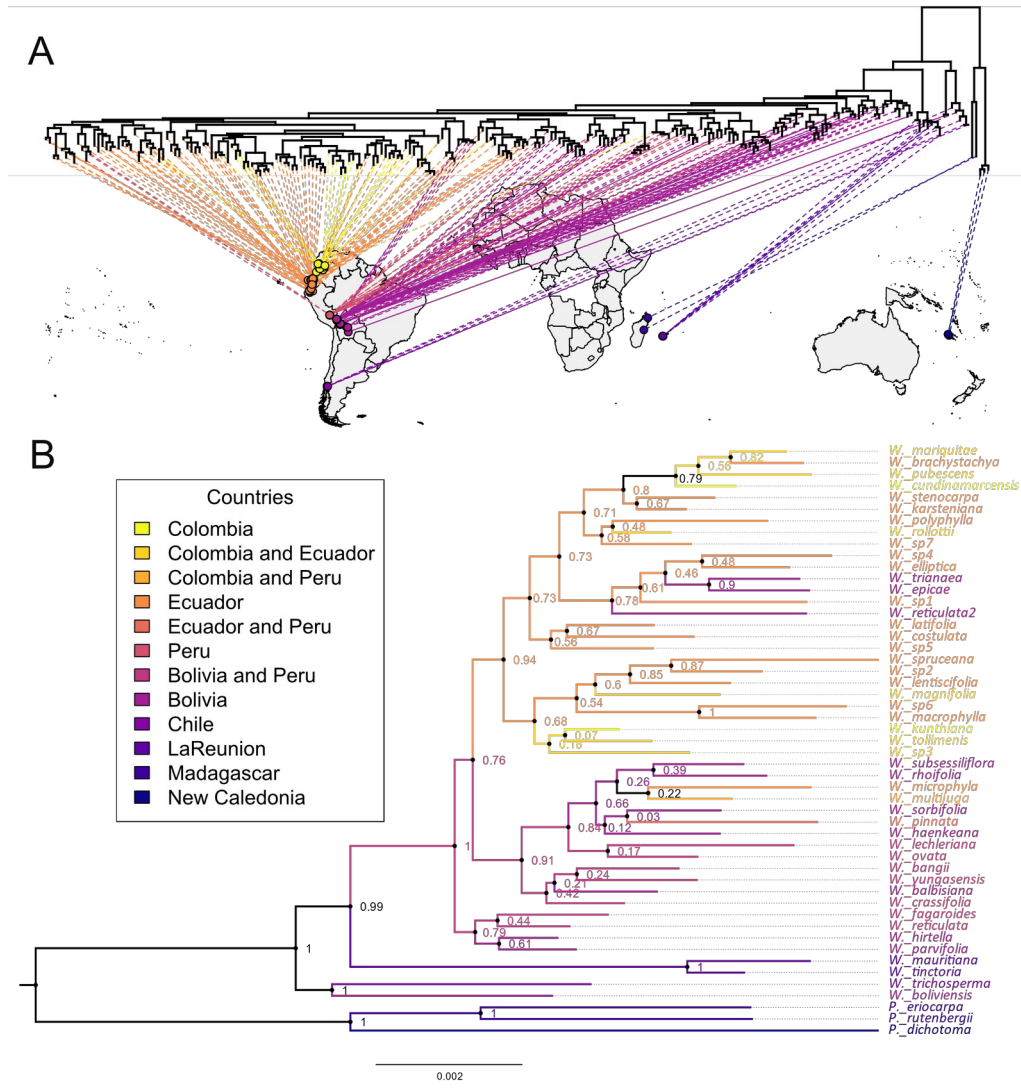


**Figure 1. Geographic structure of phylogenetic (ML tree) relationships in *Weinmannia*.** A. Specimen-level phylogeny with tips projected onto geographic locations. B. Species-level phylogeny for *Weinmannia*. Bootstrap support values are shown as node labels, tip labels and branches are colored by country where species were collected.

388  
 389  
 390  
 391  
 392  
 393  
 394

### 3.2. Species-level phylogeny 395

The character matrix for the species-tree reconstruction contained 396  
103,676 bp (2,879 loci), with 48.63% missing data, for 51 taxa. 397

The concatenated ML species tree (ML; Fig. 1B;) and the multi- 398  
species coalescent model-based species tree (hereafter SVDQ tree; 399

Supplementary Fig. 3) both showed strong bootstrap support 400

[Bootstrap Support (BS) = 1 in both cases] for genus *Weinmannia*, 401

confirming its monophyly. The time-calibrated phylogeny based on 402

the ML topology showed that the MRCA of *Weinmannia* diverged 403

from the outgroup in the late Eocene around 34.4 Ma and started to 404

diversify ~20.7 Ma (Fig. 2), with similar results observed in the 405

SVDQ tree analysis (~21.38 Ma; Supplementary Fig. 4). Congruent 406

with our specimen-level phylogeny, the species-level phylogenies 407

also showed a general trend where geographically proximal taxa 408

were found in the same clade (Fig. 1B; Supplementary Figs. 1,2). 409

In the ML species tree, *Weinmannia trichosperma*, the 410

southernmost species located in the temperate, extratropical forests 411

of southern South America, was placed in a clade that was strongly 412

supported as the sister group to the remaining species of 413

*Weinmannia* (BS = 1; Fig. 1B), along with *Weinmannia boliviensis* 414

R.E.Fr., the southernmost species in the central Andes inhabiting 415

the subtropical Tucuman-Bolivian forests. The ML phylogeny also 416

shows that *W. trichosperma* and *W. boliviensis* diverged from each other 17.9 Ma, which is older than the onset of diversification in the tropical Andean clade, which is dated at 13.8 Ma (Fig. 2). In contrast, our SVDQ tree shows a topology with *W. boliviensis*, a clade consisting of the two Mascarene species, and then *W. trichosperma* as successive sister groups to the remaining *Weinmannia* species (supplementary Figs. 2 and 3). Despite the topological differences between these two trees, both strongly support the placement of the southernmost lineages *W. trichosperma* and *W. boliviensis*, alongside *W. mauritiana* and *W. tinctoria*, as sister lineages to the remainder of *Weinmannia* in the phylogeny.

417  
418  
419  
420  
421  
422  
423  
424  
425  
426  
427  
428  
429

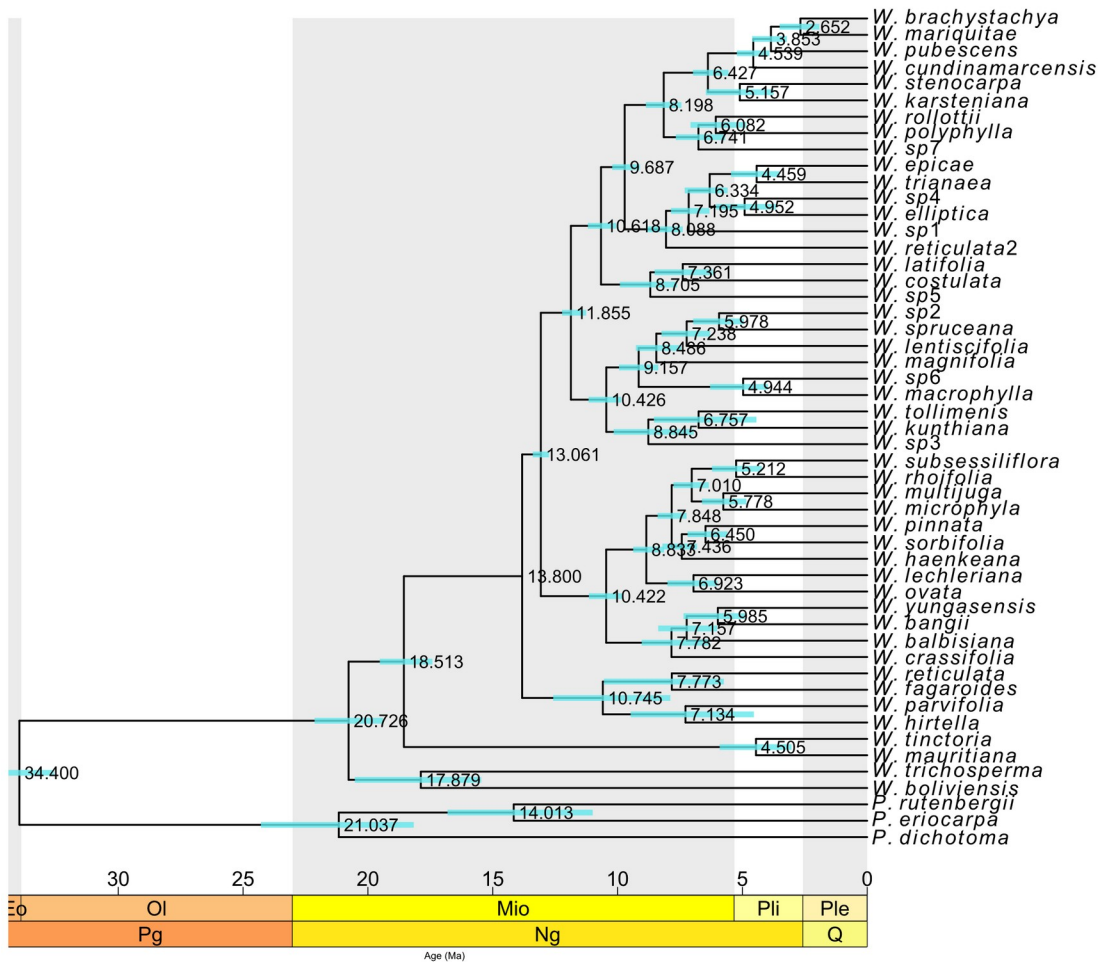


**Figure 2. Maximum likelihood phylogeny with estimated divergence times of *Weinmannia* species.** Median divergence age estimates across bootstrap trees with 95% confidence intervals in blue bars.

430  
431  
432  
433  
434  
435

**3.3. The tropical Andean clade shows geographic structure in the Central and Northern Andes.** After the divergence of *Weinmannia* in southern South America and the Mascarenes, the

436  
437  
438

remaining 44 species, which are found exclusively in the tropical 439  
Andes, formed a large, strongly supported clade (BS=1 in Fig. 1B 440  
for ML; and BS= 0.98 in Supplementary Fig. 2 for SVDQ), which 441  
started to diversify ~13.8 Mya (Fig. 2 and Supplementary Fig. 4). 442  
Even accounting for the topological differences between the SVDQ 443  
and ML trees (Supplementary Fig. 3), the Tropical Andean clade 444  
exhibited clear geographic structure. The ML reconstruction shows 445  
two clades at its base, the first containing four species from Bolivia 446  
and Peru (BS= 0.79; Fig. 1B), and its sister clade (BS=0.76; Fig. 447  
1B), which bifurcated into two major clades. The first of these 448  
clades was strongly supported (BS=0.91; Fig. 1B) and included 13 449  
species from the central Andes, with exceptions such as 450  
*Weinmannia multijuga* Killip & A. C. Sm. from Peru and 451  
Colombia, *Weinmannia pinnata* L. from Peru and Ecuador, and 452  
*Weinmannia microphylla* Ruiz & Pav. from Ecuador. The second of 453  
these clades was also well supported (BS = 0.84; Fig. 1B) and 454  
included most species from the northern Andes (Ecuador and 455  
Colombia), except for *Weinmannia trianaea* Wedd., *Weinmannia* 456  
*epicae* A. Fuentes, and what we call *Weinmannia reticulata*<sup>2</sup> from 457  
Bolivia (Fig. 1B). 458

Our SVDQuartets species tree showed a similar pattern for 459  
the Tropical Andes clade, in that it was divided into two major 460



clades. The first contained 16 species, all found in the central  
Andes of Bolivia and Peru, except for *W. multijuga*, which is found  
from Colombia to Peru (BS= 0.83, Supplementary Fig. 2). The  
second clade was well supported (BS=0.84) and contained the  
remaining 28 species, all from the northern Andes except *W.*  
*reticulata2* and *W. balbisi* Kunth from Bolivia (Supplementary  
Fig. 2).

### **3.4. Younger clades are distributed towards northern latitudes.**

Ancestral state reconstructions for latitudes in internal nodes of the  
phylogeny for American species show that nodes with older  
divergence times are more likely to be associated with more  
southern reconstructed latitudes. Likewise, nodes with younger  
divergence times are more likely to be associated with more  
northern reconstructed latitudes (Fig. 3A and Supplementary Fig.  
5A).

Our Bayesian model predicting node age as a function of  
reconstructed latitude on the ML phylogeny yielded a maximum *a*  
*posteriori* (MAP) slope for latitude ( $\beta$ ) of -0.486. The 99% credible  
interval estimated for this parameter ranged from -0.795 to -0.201,  
which does not include zero, providing robust evidence to reject the

null hypothesis ( $\beta=0$ ; Fig. 3C) of no relationship between node age 482  
and latitude. Using our SVDQ topology with ML-optimized branch 483  
lengths we observed identical results where nodes with shorter 484  
distance from the root tended to be associated with more southern 485  
latitudes (MAP for slope = -0.337; Supplementary Fig. 5C), with 486  
the null hypothesis rejected with a 99% credible interval ranging 487  
from -0.555 to -0.0975 (Supplementary Fig. 5C). Accordingly, the 488  
results of the NHST with nonparametric bootstrap on the slope 489  
coefficient also showed that node age tended to be negatively 490  
related to ancestral latitude when using both our ML tree topology 491  
(slope =  $-0.481 \pm 0.101$ ;  $p$ -value = 0.00000, Supplementary Fig. 6A) 492  
and SVDQ topology (slope =  $-0.315 \pm 0.074$ ;  $p$ -value = 0.00002, 493  
Supplementary Fig 6B). Likewise, we obtained equivalent results 494  
for both ML and SVDQ topologies and statistical methods when 495  
we included the two Mascarene species in the analysis 496  
(Supplementary Figs. 6C,6D and Supplementary Figs. 7,8). 497

498

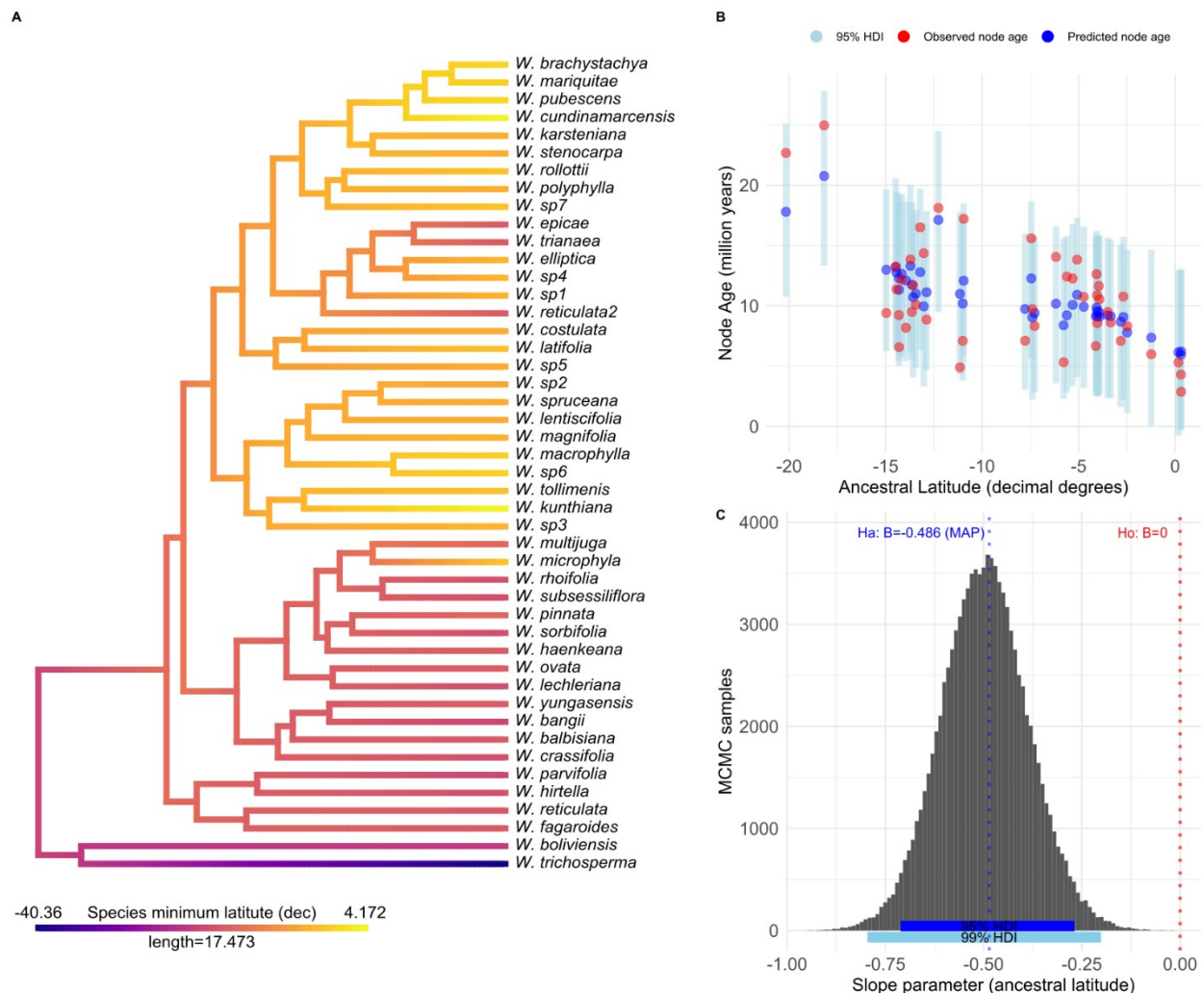


**Figure 3. Analyses of migration from southern latitudes to the northern Andes using ML topology, excluding Mascarene species.** A. Ancestral character reconstruction for latitude of hypothetical ancestors (nodes). The colors depict a continuous gradient of latitude, transitioning from southern temperate regions in blue to northern tropical regions in yellow, with intermediate latitudes in the central Andes represented in red. B. Bayesian linear regression of node age as a function of predicted ancestral latitude. Observed values are represented in red dots. The blue dots represent the maximum a posteriori estimates and the sky blue bars represent 95% High Density Intervals (HDI) of model-generated node ages. C. A posteriori probability distribution for the estimated slope coefficient for latitude as a predictor of node age.

### 3.5. Despite variation in elevation and latitude, the

extratropical temperature niche remained stable. Results of

ancestral character reconstruction showed that the mean annual

499  
 500  
 501  
 502  
 503  
 504  
 505  
 506  
 507  
 508  
 509  
 510  
 511

temperature (BIO 1) changed very little across phylogeny in relation to the MRCA of *Weinmannia* species, with values generally remaining similar to those found in the MRCA of the *trichosperma-boliviensis* clade, especially for older nodes (Supplementary Fig. 9A and D). Accordingly, the wald-test showed that the mean  $d_{root}$  estimate for mean annual temperature was not statistically different from zero ( $d_{root}=-0.00235$ ,  $P=0.172$ , Fig. 4, Supplementary Table 1). In contrast, reconstructed ancestral elevation and latitude showed greater changes over evolutionary time (Supplementary Fig. 9B-C), with both showing positive  $d_{root}$  values that were statistically different from zero (mean  $d_{root}$  values of 0.0193,  $P<0.0001$  and 0.0251,  $P<0.0001$ , respectively). These results indicated that species shifted away from the MRCA of the extant extratropical lineage (containing *trichosperma-boliviensis*) towards higher elevations and higher (northern) latitudes over evolutionary time. Likelihood ratio test against the null model assuming no differences (deviance=0.0192,  $df_1=137$ ,  $df=135$ ,  $P < 0.000001$ ) and Paired t-test comparisons for  $d_{root}$  means (Fig. 4) showed statistically significant differences in  $d_{root}$  between all three reconstructed variables. Smaller rates of change values for BIO1 relative to elevation and Latitude suggest conservatism of the thermal niche. Further, regression analysis of the  $d_{root}$  metric as a

function of node depth also supports the notion of thermal niche 534  
stability across phylogenetic scales (slope = 0.00001, P = 0.95), as 535  
opposed to elevation (slope = 0.00043, P < 0.05) and latitude (slope 536  
= 0.00048, P < 0.05), which displayed positive slopes significantly 537  
different that zero, reflecting more evolutionary changes at deeper 538  
nodes (Supplementary Fig. 9D-F). 539

540

541

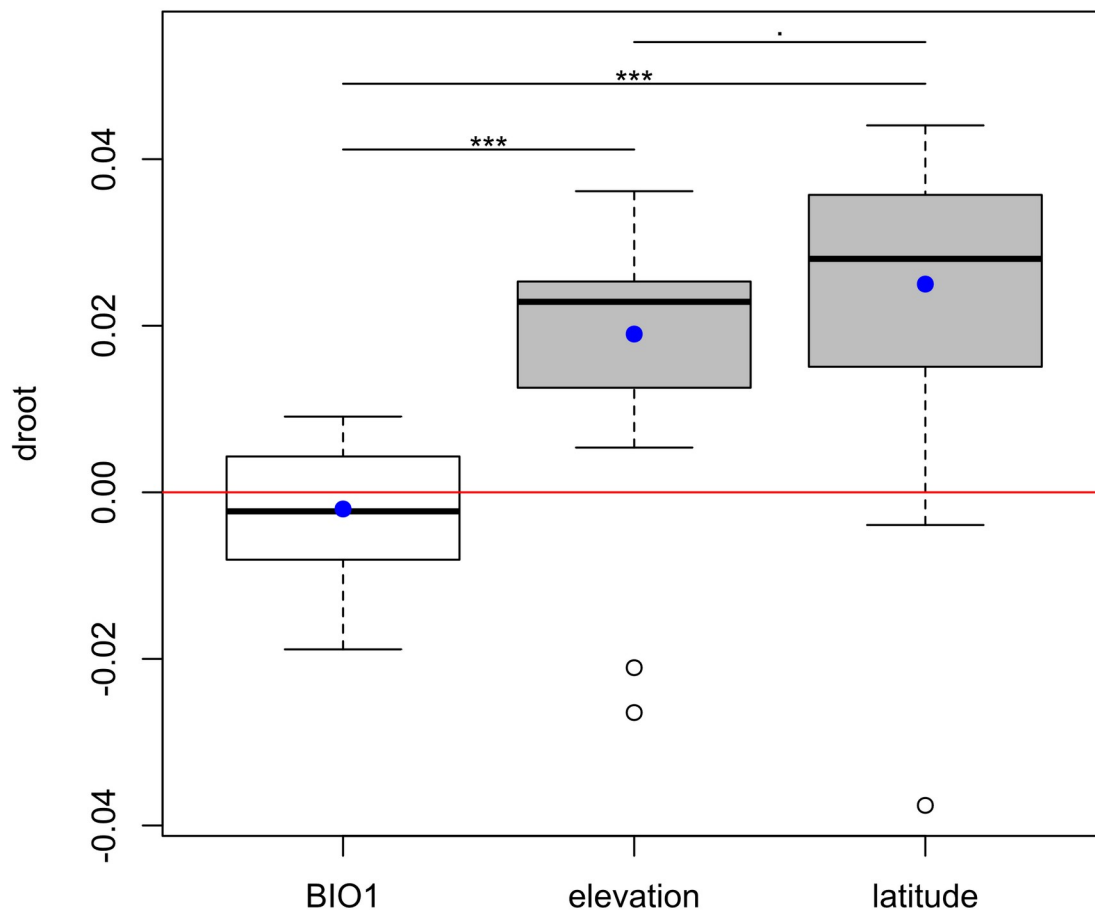


**Figure 4.** Comparison of evolutionary rates ( $d_{root}$ ) from each node to the MRCA of *Weinmannia*. 543  
Boxplots show  $d_{root}$  values for ancestral reconstructions of mean annual temperature (BIO1), 544  
elevation, and latitude. White boxes indicate variables with  $d_{root}$  values not significantly different 545  
from 0 ( $p>0.05$ ) and gray boxes indicate significant differences ( $p<0.05$ ) based on a wald-test. 546  
Blue dots represent the mean  $d_{root}$  for each variable. Pairwise t-test comparisons are shown with 547  
lines above the boxes, with significance levels: ns>0.05, .<0.05, \*<0.01, \*\*<0.001, \*\*\*<0.0001. 548

549

## 4. Discussion

550

Our analyses of *Weinmannia* reveal that extratropical 551  
species were placed at the base of the phylogeny, although the 552  
origin and early diversification of the clade remain equivocal. We 553  
also find a robust negative relationship between the age of clades 554  
and their latitudinal distribution across the phylogeny, suggesting a 555  
south-to-north dispersal route. We also found that the clade exhibits 556  
strong thermal niche conservatism despite showing large changes 557  
in elevation and latitude. These results are consistent with the 558  
hypothesis that *Weinmannia* may have originated from a lineage 559  
that was pre-adapted to the climatic conditions of the southern 560  
extratropics, and that the arrival and diversification of *Weinmannia* 561  
in the American tropics occurred when suitable climates were 562  
created as a result of the Andean uplift. 563

564

### 4.1. An extratropical origin for *Weinmannia*

565

Our ML phylogeny places *Weinmannia trichosperma* from 566  
the temperate forests of southern South America in a clade that is 567  
sister to all other species of *Weinmannia* (ML, BS = 1, Fig. 1). This 568  
is consistent with previous morphological and genetic 569  
reconstructions of the phylogenetic relationships of species in the 570  
genus (Bradford, 1998, 2002), but is slightly different from results 571  
with our SVDQ approach (Supplementary Fig. 2). Also 572  
consistently placed among the oldest diverging lineages is the 573  
subtropical species *Weinmannia boliviensis* (Fig. 1a and S2). *W.* 574  
*boliviensis* is distributed in the Tucuman-Bolivian forests (Harling 575  
and Fuentes, 2014), which are subtropical montane forests on the 576  
eastern slope of the Andes, extending from 23°S to 29°S (Cabrera, 577  
1976). According to our ML phylogeny, *W. boliviensis* and *W.* 578  
*trichosperma* diverged during the Miocene, older than the ancestral 579  
node for the tropical species (~17.9 Ma. Fig. 2). Furthermore, this 580  
date precedes the final uplift of the central and southern Andes to 581  
their present elevations (above 3000 m), which began during the 582  
late Miocene (~11 Ma) (Gregory-Wodzicki, 2000; Siravo et al., 583  
2018), and the subsequent expansion of arid areas to the west and 584  
east of the mountain range (the southern arid diagonal of South 585  
America; Rambo, 1952). Therefore, the evolutionary divergence of 586  
the base of *Weinmannia* would have occurred in forests composed 587

of Gondwanan lineages that persisted in South America during the 588  
Paleogene and Neogene (Romero, 1986), which were deeply 589  
isolated from the tropical lowland flora by environmental rather 590  
than geographic factors (Jaramillo and Cárdenas, 2013) and 591  
accumulated their own evolutionary uniqueness (Segovia et al., 592  
2020). 593

The topology with a basal subtropical and extratropical 594  
lineage is consistent with three possible biogeographic scenarios 595  
for the origin and early evolution of *Weinmannia* in South America. 596  
The first is that an extratropical *Weinmannia* originated or initially 597  
colonized southern South America and diversified northward as the 598  
climate in tropical America became more suitable following the 599  
Andean uplift. The second is that *Weinmannia* originated in lower 600  
latitudes of America and experienced an early divergence, with one 601  
lineage dispersing to the south and giving rise to *W. trichosperma* 602  
and *W. boliviensis*, and one staying and diversifying together with 603  
the central Andes uplift, later diversifying northward into the 604  
tropical Andes once suitable habitat became available following the 605  
uplift of the northern Andes. The third is that the common ancestor 606  
of *Weinmannia* first colonized South America, expanded its 607  
distribution into both the high and low latitudes, and then 608  
experienced a vicariance event that led to the formation of the 609



southern Andes and tropical Andes clades, followed by extensive 610  
diversification in the Tropical Andes clade as habitats became 611  
suitable following the uplift of the Andes. Regardless of exactly 612  
how the origin and early diversification of *Weinmannia* occurred, 613  
many different lines of evidence support the hypothesis that 614  
*Weinmannia* represents an extratropical lineage that diversified 615  
northward only once suitably environments became available due 616  
to the uplift of the Andes. 617

The hypothesis of an extratropical origin of *Weinmannia* is 618  
consistent with paleontological evidence indicating that the lineage 619  
had a widespread distribution in the southern extratropics during 620  
the Paleogene. For example, an early Oligocene (~30 Ma) 621  
macrofossil record, *Weinmanniaphyllum bernardii* R.J. Carp. & 622  
A.M. Buchan from extratropical Tasmania (Carpenter and 623  
Buchanan 1993), where the genus is now extinct, is 624  
morphologically similar to *W. trichosperma* (Bradford, 1998). The 625  
extinction of *Weinmannia* outside of its modern range in the 626  
Americas and the Mascarenes may be related to a sharp reduction 627  
in forest cover due to the formation of the Antarctic Ice Sheet in the 628  
early Oligocene, which was associated with a massive extinction of 629  
the Austral paleoflora across the southern hemisphere (Francis, 630  
1996; Truswell and Macphail, 2009). Later, *Weinmannia* species 631

inhabiting the American extratropics would have experienced a 632  
new process of extinction as a result of the intensification of aridity 633  
triggered by the Andean orogeny, leaving remnants in specific 634  
locations along the Pacific coast of southern South America, on the 635  
Brazilian plateau, and on the slopes of the tropical Andean 636  
mountain range. This massive extinction process may also explain 637  
why the clade containing *W. trichosperma* and *W. boliviensis* is 638  
currently relatively poor in species richness (Fig. 1, 2), despite 639  
showing evidence of having a wider geographic distribution in the 640  
past (Antonelli and Sanmartín, 2011b). 641

642

#### **4.2. South-to-North dispersal and thermal niche conservatism 643 through the Andean Corridor 644**

The robust negative relationship between node age and 645  
latitude in our phylogeny reveals a late arrival of the lineage in the 646  
tropics and a south-to-north dispersal route along the Andes (Fig. 3 647  
and Supplementary Figs. 5 and 6). This scenario is consistent with 648  
fossil evidence showing that the oldest pollen records of 649  
*Weinmannia* in the northern Andes are from the late Pliocene and 650  
Pleistocene (1.5–3.2 Ma) (Van der Hammen et al., 1973). The 651  
crown age of the Northern Andes clade recovered in the present 652

study is estimated at 11.9 Ma (Fig. 2), predating the earliest fossil 653  
evidence for *Weinmannia* in the region by several million years. 654  
This inconsistency may be due to the low preservation potential of 655  
the pollen or sampling intensity in the fossil record, which can 656  
cause the date of first fossil appearance to be significantly younger 657  
than the true arrival date of a taxon in a region (Smith and Peterson, 658  
2002). 659

The phylogenies generated in this study have provided 660  
strong evidence for the direction of the dispersal of *Weinmannia*, 661  
even though tree topologies differed somewhat between RAxML 662  
and SVDQ. These differences in phylogenetic tree topologies when 663  
using SVDquartet and RAxML (Supplementary Fig. 3) may be due 664  
to their different underlying principles and methodologies. 665  
SVDquartets uses a quartet-based approach that relies on gene 666  
coalescence patterns without imposing specific evolutionary 667  
models, allowing it to account for complex evolutionary signals 668  
such as incomplete lineage sorting or hybridization. In contrast, 669  
RAxML is a maximum likelihood-based method that operates 670  
under defined evolutionary models to estimate relationships and 671  
branch lengths, potentially yielding a simpler tree structure. Despite 672  
the differences in methods, the overarching patterns remain robust 673  
across phylogenetic reconstruction approaches, with both 674

SVDquartets and RAxML revealing similar geographic structures. 675  
Both methods consistently identified a clade containing nearly all 676  
species from the northern Andes nested within a broader clade 677  
containing all species from the tropical Andes (Fig. 1 and 678  
Supplementary Fig. 2). Although the trees show slight differences 679  
in statistical support, the robust trend of northern lineages 680  
appearing more recently suggests that lineage dispersal likely 681  
followed a northward progression through the Andes (Fig. 3 and 682  
Supplementary Figs. 5 and 6). 683

Given the south-to- north dispersal route, the high thermal 684  
niche conservatism found in *Weinmannia* (Fig. 4 and 685  
Supplementary Fig. 9) suggests that the lineage first evolved under 686  
the environmental conditions of the southern extratropics and 687  
maintained these adaptations during south-to-north dispersal. Our 688  
results show that the MRCA of *Weinmannia* likely occupied a 689  
niche with relatively cool mean annual temperatures 690  
(Supplementary Fig. 9). This extratropical niche has remained 691  
stable throughout the evolutionary history of the clade, with 692  
ancestral Mean annual temperature (BIO1) showing little change 693  
across the phylogeny (Fig 4 and Supplementary Fig. 9A and D). In 694  
contrast, larger changes observed in elevation and latitude reflect 695  
the dynamic nature of *Weinmannia's* elevational shifts, as lineages 696

moved to higher elevations and latitudes over evolutionary time 697  
(Fig 4 and Supplementary Fig. 9B-C and E-F ). Plant lineages often 698  
exhibit a high degree of phylogenetic niche conservatism (Crisp et 699  
al., 2009), and this tendency to maintain a stable thermal niche 700  
likely allowed *Weinmannia* and other extratropical lineages to 701  
rapidly colonize the similar environments created at mid- and high 702  
elevations following the uplift of the Andes at tropical latitudes 703  
(Donoghue, 2008; Segovia and Armesto, 2015). This is consistent 704  
with the notion that pre-adapted clades like *Weinmannia* followed 705  
their temperature preferences during dispersal, while 706  
simultaneously adjusting to the varied elevations encountered in 707  
tropical mountain ecosystems. These results support the idea that 708  
ecological sorting of pre-adapted clades had a significant influence 709  
in shaping Andean tree communities (Ramírez et al., 2019; 710  
Griffiths et al., 2020; Linan et al., 2021a). 711

Our analyses that showed thermal niche stability across the 712  
phylogeny despite changes in elevation and latitude also support 713  
the idea that an environmental corridor facilitated environmentally 714  
driven immigration of plant lineages into the tropical Andes. One 715  
particular environmental factor that may play an important role in 716  
defining this corridor is the presence of freezing temperatures. It 717  
has been suggested that freezing temperatures drive taxonomic 718

turnover and differentiate lower and higher elevation montane 719  
forests in the northern Andes (Pérez-Escobar et al., 2022). An 720  
analysis of phylogenetic similarities of tree assemblages along the 721  
Americas also supported the idea of biological corridor that is 722  
differentiated by whether freezing temperatures occur regularly 723  
(Segovia et al., 2020). Therefore, the current taxonomic and 724  
phylogenetic turnover, and thus the historical corridor shaped by 725  
freezing temperatures in the tropical Andes, may exemplify the 726  
global pattern of conservative evolution of frost tolerance in plants 727  
(Wiens and Donoghue, 2004, Zanne et al., 2014). 728

729

#### **4.3. The intriguing history of the Mascarenes' *Weinmannia*** 730

Both our ML and SVDQ phylogenies show that a small 731  
clade containing two species from the western Indian Ocean, 732  
*Weinmannia tinctoria* Sm. and *Weinmannia mauritania* D.Don, is 733  
nested within South American *Weinmannia* (Fig. 1 and 734  
Supplementary Fig. 2), which confirms previous phylogenetic 735  
reconstructions (Bradford, 2002). This result is surprising because 736  
it implies a long-distance dispersal event, but with the stem age 737  
(~18.513 Ma, Fig. 2 and ~ 19.749 Ma, Supplementary Fig. 4) of the 738  
Mascarene clade older than the volcanic origin of the archipelago 739

(less than 8 Ma, McDougall and Chamalaun, 1969). Furthermore, 740  
this result is unusual because botanical affinities and phylogenetic 741  
evidence suggest that Madagascar may have acted as a source of 742  
diversity for the Mascarenes (Linan et al., 2019), but no species of 743  
*Weinmannia* are currently found in Madagascar or Africa (Pillon et 744  
al., 2021). Thus, any model for the dispersal of *Weinmannia* from 745  
South America can only be proposed if Madagascar or Africa are 746  
involved as a cryptic stepping-stone to reach the Mascarenes. In 747  
any case, further studies are needed to properly address this 748  
intriguing disjunction and to clarify possible vicariant or long- 749  
distance dispersal events in the origin of the genus *Weinmannia*. 750

751

## 5. Conclusion 752

*Weinmannia* reflects a pattern in which a lineage of 753  
potentially extratropical origin shows lower species richness in the 754  
extratropics than in the recently colonized tropics. This pattern, 755  
likely due to massive extratropical extinctions and recent 756  
diversification as suitable habitat became available in the tropics 757  
due to the uplift of the Andes, has also been proposed for the entire 758  
family Cunoniaceae (Pillon et al., 2021), which has traditionally 759  
been considered a lineage derived from the "Gondwanan" center of 760

plant diversification (Raven and Axelrod, 1974). Furthermore, the fossil record indicates that the Cunoniaceae family was present in Antarctica (i.e., western Gondwana) during the Late Cretaceous (~70 Ma), along with a highly diverse vegetation similar in taxonomic composition to the temperate forests of southern South America today (Poole et al., 2003). This suggests that the biogeographic history of *Weinmannia* and Cunoniaceae may have been shared with other lineages from the so-called Austral Floristic Realm (Segovia and Armesto, 2015), which likely served as an important source of biodiversity contributing to the hyperdiversity of plants in the Andes.

### **Acknowledgements**

The study was supported by FONDECYT 11200967 and the National Science Foundation (DEB 1836353). R.A.S is supported by Institute of Ecology and Biodiversity (IEB) ANID grant FB210006, F.F.G. was supported by the Shirley A. Graham Fellowships in Systematic Botany and Biogeography of the Missouri Botanical Garden. C.E.E. and the Conservation Genetics Program at the Missouri Botanical Garden is supported by donations from Stephen and Camilla Brauer, Philip and Sima



Needleman, and the Bellwether Foundation. Collections in Ecuador 782  
were partially funded by Universidad Tecnológica Indoamérica, 783  
NHO. We thank the Ministerio del Ambiente, Agua y Transición 784  
Ecológica in Ecuador for collecting permits (contrato marco MAE- 785  
DNB-CM-2019-011). 786

787

### References 788

- Acha S., Linan A., MacDougal J., Edwards C. 2021. The 789  
evolutionary history of vines in a neotropical biodiversity 790  
hotspot: Phylogenomics and biogeography of a large passion 791  
flower clade (*Passiflora* section *Decaloba*). *Mol.* 792  
*Phylogenetics Evol.* 164:107260. 793
- Antonelli A., Sanmartín I. 2011a. Why are there so many plant 794  
species in the Neotropics? *Taxon* 60:403–414. 795
- Antonelli A., Sanmartín I. 2011b. Mass extinction, gradual cooling, 796  
or rapid radiation Reconstructing the spatiotemporal 797  
evolution of the ancient angiosperm genus *Hedyosmum* 798  
(Chloranthaceae) using empirical and simulated approaches. 799  
*Syst. Biol.* 60:596–615. 800

Antonelli A., Zizka A., Silvestro D., Scharn R., Cascales-Miñana B.,	801
Bacon C. D. 2015. An engine for global plant diversity:	802
highest evolutionary turnover and emigration in the	803
American tropics. <i>Frontiers in Genetics</i> 6:130.	804
Bacon C.D., Velásquez-Puentes F.J., Hinojosa L.F., Schwartz T.,	805
Oxelman B., Pfeil B., Arroyo M.T.K., Wanntorp L.,	806
Antonelli A. 2018. Evolutionary persistence in <i>Gunnera</i> and	807
the contribution of southern plant groups to the tropical	808
Andes biodiversity hotspot. <i>PeerJ</i> 6: e4388.	809
Balslev H. 1993. Introduction. In: Balslev H., editor, <i>Neotropical</i>	810
<i>Montane Forests – Biodiversity and Conservation</i> . Aarhus,	811
Denmark: AUU Reports 31, Aarhus University Press.	812
Berry E.W. 1917. The Age of the Bolivian Andes. <i>Proc. Natl. Acad.</i>	813
<i>Sci. U.S.A.</i> 3:283–285.	814
Bradford J.C. 1998. A cladistic analysis of species groups in	815
<i>Weinmannia</i> (Cunoniaceae) based on morphology and	816
inflorescence architecture. <i>Ann. Missouri Bot. Gard.</i> 85:565-	817
593.	818
Bradford J.C. 2002. Molecular phylogenetics and morphological	819
evolution in Cunoniaceae (Cunoniaceae). <i>Ann. Missouri Bot.</i>	820
<i>Gard.</i> 89:491-503.	821

Bradford J. C., Fortune-Hopkins H. C. Barnes R. W. 2004	822
<i>Cunoniaceae</i> . In The families and genera of vascular plants	823
(ed. K. Kubitzki), pp. 91–111. Heidelberg, Germany:	824
Springer.	825
Cabrera A.L. 1976. Regiones fitogeográficas argentinas.	826
<i>Enciclopedia Argentina de Agricultura y Jardinería</i> 2:1-85.	827
Carpenter R.J., Buchanan A.M. 1993. Oligocene leaves, fruit and	828
flowers of the Cunoniaceae from Cethana, Tasmania. <i>Aust.</i>	829
<i>Syst. Bot.</i> 6:91-109.	830
Carpenter B., Gelman A., Hoffman M.D., Lee D., Goodrich B.,	831
Betancourt M., Brubaker M., Guo J., Li P., Riddell A. 2017.	832
Stan: A Probabilistic Programming Language. <i>J. Stat. Soft.</i>	833
76:1–32.	834
Chacón, J., de Assis, M. C., Meerow, A. W., Renner, S. S. 2012.	835
From east Gondwana to Central America: historical	836
biogeography of the Alstroemeriaceae. <i>Journal of</i>	837
<i>Biogeography</i> : 39(10), 1806-1818.	838
Chifman J., Kubatko L. 2014. Quartet Inference from SNP Data	839
Under the Coalescent Model. <i>Bioinformatics</i> : 30:3317–3324.	840

Crisp M. D., Arroyo M. T., Cook L. G., Gandolfo M. A., Jordan G.	841
J., McGlone M. S., Weston P.H., Westoby M., Wilf P., et al.	842
2009. Phylogenetic biome conservatism on a global scale.	843
<i>Nature</i> 458: 754-756.	844
Donoghue M.J. 2008. A phylogenetic perspective on the distribution	845
of plant diversity. <i>Proc. Natl. Acad. Sci.</i> 105:11549-11555.	846
Doyle J.J., Doyle J.L. 1987. A rapid DNA isolation procedure for	847
small quantities of fresh leaf tissue. <i>Phytochem. Bull.</i> 19:11–	848
15.	849
Drummond A. J. Rambaut A.2007. BEAST: Bayesian evolutionary	850
analysis by sampling trees. <i>BMC Evol. Biol.</i> 7:214.	851
Earl D.A., von Holdt B.M. 2012. STRUCTURE HARVESTER: a	852
website and program for visualizing STRUCTURE output	853
and implementing the Evanno method. <i>Conserv. Genet.</i>	854
<i>Resour.</i> 4: 359-361.	855
Eaton D.A.R., Overcast I. 2020. ipyrad: interactive assembly and	856
analysis of RADseq datasets. <i>Bioinformatics.</i> 36:2592–2594.	857
Fick S.E., Hijmans R.J. 2017. WorldClim 2: new 1-km spatial	858
resolution climate surfaces for global land areas.	859
<i>International Journal of Climatology</i> 37, 4302–4315.	860

Francis J.E. 1996. Antarctic palaeobotany: clues to climate change.	861
<i>Terra Antarctica</i> 3:135–140.	862
González-Caro S., Tello J.S., Myers J.A., Feeley K., Blundo C.,	863
Calderón-Loor M., Carilla J., Cayola L., Cuesta F., Farfán	864
W., et al. 2023. Historical Assembly of Andean Tree	865
Communities. <i>Plants</i> 12:3546.	866
Graham, A. 1973. History of the arborescent temperate element in	867
the northern Latin American biota. <i>Vegetation and</i>	868
vegetational history of northern Latin America, 301-314.	869
Graham, A. 1995. Development of affinities between	870
Mexican/Central American and northern South American	871
lowland and lower montane vegetation during the Tertiary.	872
Pp. 11-22 in S. P. Churchill, H. Balslev, E. Forero & J. L.	873
Luteyn (editors), <i>Biodiversity and Conservation of</i>	874
Neotropical Montane Forests. New York Botanical Garden,	875
Bronx.	876
Graham A., Gregory-Wodzicki K.M., Wright K.L. 2001. Studies in	877
Neotropical Paleobotany. XV. A Mio-Pliocene palynoflora	878
from the Eastern Cordillera, Bolivia: implications for the	879
uplift history of the Central Andes. <i>American Journal of</i>	880
<i>Botany</i> 88, 1545–1557.	881

Gregory-Wodzicki K.M. 2000. Uplift history of the Central and	882
Northern Andes: a review. <i>Geol. Soc. Am. Bull.</i> 112:1091-	883
1105.	884
Griffiths A.R., Silman M.R., Farfán Rios W., Feeley K.J., García	885
Cabrera K., Meir P., Salinas N., Dexter K.G. 2020.	886
Evolutionary heritage shapes tree distributions along an	887
Amazon-to-Andes elevation gradient. <i>Biotropica</i> 53:38–50.	888
Haldane J.B.S. 1949. Suggestions as to Quantitative Measurement	889
of Rates of Evolution. <i>Evolution</i> 3, 51–56.	890
Harling G.W. Fuentes A.F. 2014. Cunoniaceae. In: P.M. Jørgensen,	891
M.H. Nee, S.G. Beck, editors. <i>Cat. Pl. Vasc. Bolivia,</i>	892
<i>Monogr. Syst. Bot. Missouri Bot. Gard.</i> 127. St. Louis.USA.	893
Missouri Botanical Garden Press:540–542.	894
Hooghiemstra H. 1984. Vegetational and climatic history of the high	895
plain of Bogotá, Colombia: A continuous record of the last	896
3.5 million years. <i>Diss. Bot.</i> 79:368.	897
Hughes, C., & Eastwood, R. 2006. Island radiation on a continental	898
scale: exceptional rates of plant diversification after uplift of	899
the Andes. <i>Proceedings of the National Academy of</i>	900
<i>Sciences:</i> 103(27), 10334-10339.	901

Inglis P.W., Pappas M., Resende L.V., Grattapaglia D. 2018. Fast	902
and inexpensive protocols for consistent extraction of high	903
quality DNA and RNA from challenging plant and fungal	904
samples for high-throughput SNP genotyping and	905
sequencing applications. <i>PLoS ONE</i> 13: e0206085.	906
Jaramillo C., Cárdenas A. 2013. Global warming and neotropical	907
rainforests: a historical perspective. <i>Annu. Rev. Earth Pl. Sc.</i>	908
41:741–766.	909
Lemoine F., Domelevo Entfellner J.-B., Wilkinson E., Correia D.,	910
Dávila Felipe M., De Oliveira T., Gascuel O. 2018.	911
Renewing Felsenstein’s phylogenetic bootstrap in the era of	912
big data. <i>Nature</i> 556:452–456.	913
Linan A.G., Schatz G.E., Lowry P.P., Miller A., Edwards C. E.	914
2019. Ebony and the Mascarenes: the evolutionary	915
relationships and biogeography of <i>Diospyros</i> (Ebenaceae) in	916
the western Indian Ocean. <i>Bot. J. Linn. Soc.</i> 190: 359-373.	917
Linan A.G., Myers J.A., Edwards C.E., Zanne A.E., Smith S.A.,	918
Arellano G., ... Tello J. S. 2021a. The evolutionary assembly	919
of forest communities along environmental gradients: recent	920
diversification or sorting of pre-adapted clades?. <i>New Phytol.</i>	921
232(6): 2506-2519.	922

Linan A.G., Lowry II P.P., Miller A.J., Schatz G.E., Sevathian J.-C.,	923
Edwards C.E. 2021b. RAD-sequencing reveals patterns of	924
diversification and hybridization, and the accumulation of	925
reproductive isolation in a clade of partially sympatric,	926
tropical island trees. <i>Molecular Ecology</i> 30: 4520–4537.	927
Liu, B., Le, C. T., Barrett, R. L., Nickrent, D. L., Chen, Z., Lu,	928
L.,Vidal-Russell, R. 2018. Historical biogeography of	929
Loranthaceae (Santalales): Diversification agrees with	930
emergence of tropical forests and radiation of songbirds.	931
<i>Molecular Phylogenetics and Evolution</i> , 124, 199-212.	932
Luebert F., Weigend M. 2014. Phylogenetic insights into Andean	933
plant diversification. <i>Front. Ecol. Evol.</i> 2:27.	934
Mashburn B., Jhangeer-Khan R., Bégué A., Tatayah V., Olsen	935
K.M., Edwards C.E. 2023. Genetic assessment improves	936
conservation efforts for the critically endangered oceanic	937
island endemic <i>Hibiscus liliiflorus</i> . <i>J. Hered.</i> 114:259–270.	938
Maurin K.J.L. 2008. An empirical guide for producing a dated	939
phylogeny with treePL in a maximum likelihood framework.	940
McDougall I.A.N., Chamalaun F.H. 1969. Isotopic dating and	941
geomagnetic polarity studies on volcanic rocks from	942
Mauritius, Indian Ocean. <i>Geol. Soc. Am. Bull.</i> 80:1419-1442.	943



Myers N., Mittermeier R., Mittermeier C., da Fonseca G.A.B., Kent	944
J. 2000. Biodiversity hotspots for conservation priorities.	945
<i>Nature</i> 403:853–858.	946
Neves D.M., Dexter K.G., Baker T.R., Coelho de Souza F.,	947
Oliveira-Filho A.T., Queiroz, L.P., Lima H.C., Simon M.F.,	948
Lewis G.P., Segovia R.A., et al. 2020. Evolutionary diversity	949
in tropical tree communities peaks at intermediate	950
precipitation. <i>Sci. Rep.</i> 10:1188.	951
Owusu, S. A., Sullivan, A. R., Weber, J. R., Hipp, A. L., & Gailing,	952
O. 2015. Taxonomic relationships and gene flow in four	953
NorthAmerican Quercus Species (Quercus section Lobatae).	954
<i>Systematic Botany</i> , 40(2), 510–521.	955
Paradis E. & Schliep K. 2019. ape 5.0: an environment for modern	956
phylogenetics and evolutionary analyses in R.	957
<i>Bioinformatics</i> , 35, 526-528.	958
Paris J.R., Stevens J.R., Catchen J.M. 2017. Lost in parameter	959
space: a road map for stacks. <i>Methods Ecol. Evol.</i> 8:1360–	960
1373.	961
Pennington R.T., Dick C.W. 2004. The role of immigrants in the	962
assembly of the South American rainforest tree flora.	963

<i>Philosophical Transactions of the Royal Society of London.</i>	964
<i>Series B: Biological Sciences</i> 359:1611-1622.	965
Pérez-Escobar O.A., Zizka A., Bermúdez M.A., Meseguer A.S.,	966
Condamine F.L., Hoorn C., Hooghiemstra H., Pu Y.,	967
Bogarín D., Boschman L.M., Pennington R.T., et al. 2022.	968
The Andes through time: evolution and distribution of	969
Andean floras. <i>Trends Plant Sci.</i> 27:364-378.	970
Pillon Y., Hopkins H.C., Maurin O., Epiawalage, N., Bradford, J.,	971
Rogers, Z.S., Baker W.J., Forest, F. 2021. Phylogenomics	972
and biogeography of Cunoniaceae (Oxalidales) with	973
complete generic sampling and taxonomic realignments. <i>Am.</i>	974
<i>J. Bot.</i> 108:1181-1200.	975
Poole I., Mennega A.M., Cantrill D.J. 2003. Valdivian ecosystems	976
in the Late Cretaceous and Early Tertiary of Antarctica:	977
further evidence from myrtaceous and eucryphiaceous fossil	978
wood. <i>Rev. Palaeobot. Palynol.</i> 124:9-27.	979
Pritchard J.K., Stephens M., Donnelly P. 2000. Inference of	980
Population Structure Using Multilocus Genotype Data.	981
<i>Genetics</i> 155:945–959.	982
Quiroga M.P., Mathiasen P., Iglesias A., Mill R.R., Premoli A.C.	983
2016. Molecular and fossil evidence disentangle the	984

biogeographical history of Podocarpus, a key genus in plant	985
geography. <i>J. Biogeogr.</i> 43:372-383.	986
R Core Team. 2023. R: A Language and Environment for Statistical	987
Computing. R Foundation for Statistical Computing, Vienna,	988
Austria. <a href="https://www.R-project.org/">https://www.R-project.org/</a> .	989
Rahbek C., Borregaard M., Antonelli A., Colwell R., Holt B.,	990
Nogués-Bravo D., Rasmussen C., Richardson K., Rosing	991
M., Whittaker R., Fjeldså J. (2019). Building mountain	992
biodiversity: Geological and evolutionary processes. <i>Science</i>	993
365:1114-1119.	994
Rambo B. 1952. Analise geografica das compostas sul-brasileras.	995
<i>Sellowia</i> 5:87–159.	996
Ramírez S., González-Caro S., Phillips J., Cabrera E., Feeley K.J.,	997
Duque Á. 2019. The influence of historical dispersal on the	998
phylogenetic structure of tree communities in the tropical	999
Andes. <i>Biotropica</i> 51:500-508.	1000
Raven P.H., Axelrod D.I. 1974. Angiosperm biogeography and past	1001
continental movements. <i>Ann. Missouri Bot. Gard.</i> 61:539-	1002
673.	1003

Revell L.J. 2012. phytools: an R package for phylogenetic	1004
comparative biology (and other things). <i>Methods Ecol. Evol.</i>	1005
3:217–223.	1006
Romero E.J. 1986. Paleogene phytogeography and climatology of	1007
South America. <i>Ann. Missouri Bot. Gard.</i> 73:449–461.	1008
Segovia R.A., Armesto J.J. 2015. The Gondwanan legacy in South	1009
American biogeography. <i>J. Biogeogr.</i> 42:209-217.	1010
Segovia R.A., Pennington R.T., Baker T.R., Coelho de Souza F.,	1011
Neves D.M., Davis C.C., Armesto J.J., Olivera-Filho A.T.,	1012
Dexter, K. G. 2020. Freezing and water availability structure	1013
the evolutionary diversity of trees across the Americas. <i>Sc.</i>	1014
<i>Adv.</i> 6:eaaz5373.	1015
Siravo G., Fellin M.G., Faccenna C., Bayona G., Lucci F., Molin P.,	1016
Maden C. 2018. Constraints on the Cenozoic deformation of	1017
the northern Eastern Cordillera, Colombia. <i>Tectonics</i>	1018
37:4311-4337.	1019
Smith A.B., Peterson K.J. 2002. Dating the time of origin of major	1020
clades: molecular clocks and the fossil record. <i>Annu. Rev.</i>	1021
<i>Earth Planet. Sci.</i> 30: 65-88.	1022

Smith S.A., O’Meara B.C. 2012. treePL: divergence time estimation	1023
using penalized likelihood for large phylogenies.	1024
<i>Bioinformatics</i> 28:2689–2690.	1025
Stamatakis A., 2014. RAxML version 8: a tool for phylogenetic	1026
analysis and post-analysis of large phylogenies.	1027
<i>Bioinformatics</i> 30:1312–1313.	1028
Stan Development Team. 2023. RStan: the R interface to Stan. R	1029
package version 2.26.23. <a href="https://mc-stan.org/">https://mc-stan.org/</a> .	1030
Tietje M., Antonelli A., Forest F., Govaerts R., Smith S.A., Sun, M.,	1031
Baker W.J. Eiserhardt W.L. 2023. Global hotspots of plant	1032
phylogenetic diversity. <i>New Phytol.</i> 240: 1636-1646.	1033
Truswell E.M., Macphail M.K. 2009. Polar forests on the edge of	1034
extinction: what does the fossil spore and pollen evidence	1035
from East Antarctica say? <i>Aust. Syst. Bot.</i> 22:57–106.	1036
Van der Hammen T., Werner J., Van Dommelen H.1973.	1037
Palynological record of the upheaval of the Northern Andes:	1038
A study of the Pliocene and lower quaternary of the	1039
Colombian Eastern Cordillera and the early evolution of its	1040
high-Andean biota. <i>Rev. Palaeobot. Palynol.</i> 16:1–122.	1041

Wang S., Meyer E., McKay J.K., Matz M.V. 2012. 2b-RAD: a	1042
simple and flexible method for genome-wide genotyping.	1043
<i>Nat. Methods</i> 9:808–810.	1044
Wiens J.J., Donoghue M.J. 2004. Historical biogeography, ecology	1045
and species richness. <i>Trends Ecol. Evol.</i> 19:639-644.	1046
Willis J. C., H. De Vries H. B. Guppy E. M. Reid, Small J. 1922.	1047
Age and area: a study in geographical distribution and origin	1048
of species. Cambridge University Press, Cambridge.	1049
Winkworth R.C., Donoghue M.J. 2005. <i>Viburnum</i> phylogeny based	1050
on combined molecular data: implications for taxonomy and	1051
biogeography. <i>Am. J. Bot.</i> 92:653-666.	1052
Zanne A.E., Tank D.C., Cornwell W.K., Eastman J.M., Smith S.A.,	1053
FitzJohn R. G., Beaulieu J.M. 2014. Three keys to the radiation of	1054
angiosperms into freezing environments. <i>Nature</i> 506:89-92.	1055
	1056
	1057

Supplementary Material for:

**Phylogeny of *Weinmannia* (Cunoniaceae) reveals the Contribution of the Southern Extratropics to Tropical Andean Biodiversity.**

**Keywords:** immigration, diversification, hyperdiversity, tropics, Gondwana

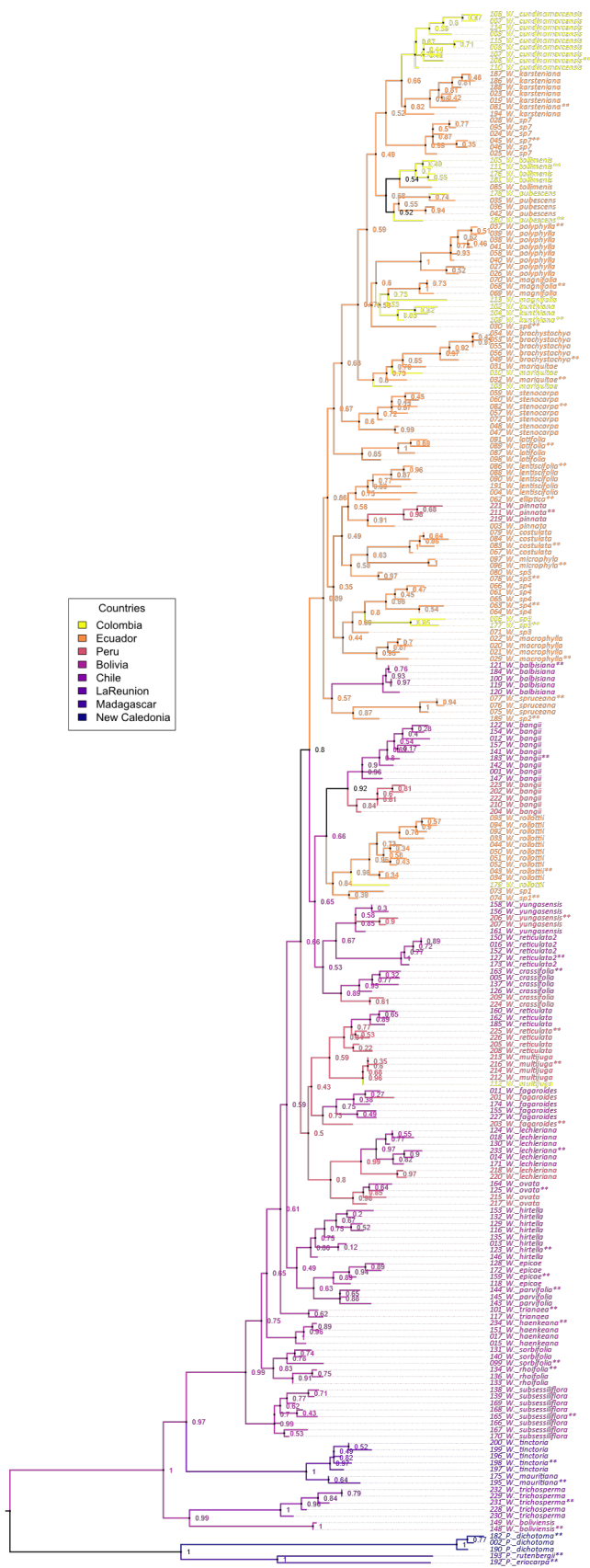
**Index**

- Supplementary Figure 1
- Supplementary Figure 2
- Supplementary Figure 3
- Supplementary Figure 4
- Supplementary Figure 5
- Supplementary Figure 6
- Supplementary Figure 7
- Supplementary Figure 8
- Supplementary Figure 9
- Supplementary Table 1
- Supplementary Methods

## Supplementary Figures

**Supplementary Figure 1:** Individual-level 2bRAD-seq tree for *Weinmannia*. Maximum Likelihood tree inferred from concatenated 2bRAD-seq data from 234 individuals of *Weinmannia* plus outgroups. Tip labels contain: First four letters of senior collector\_Collection Number/Species Name/Country abbreviation. Tips labels are colored by country of origin (see legend). Bootstrap support values are shown as branch labels next to nodes. Accessions from multiple populations of the same morphology-based species form generally well-supported clades except in the case of *W. reticulata* and *W. sorbifolia*. North Andes clade is expanded in the next page.



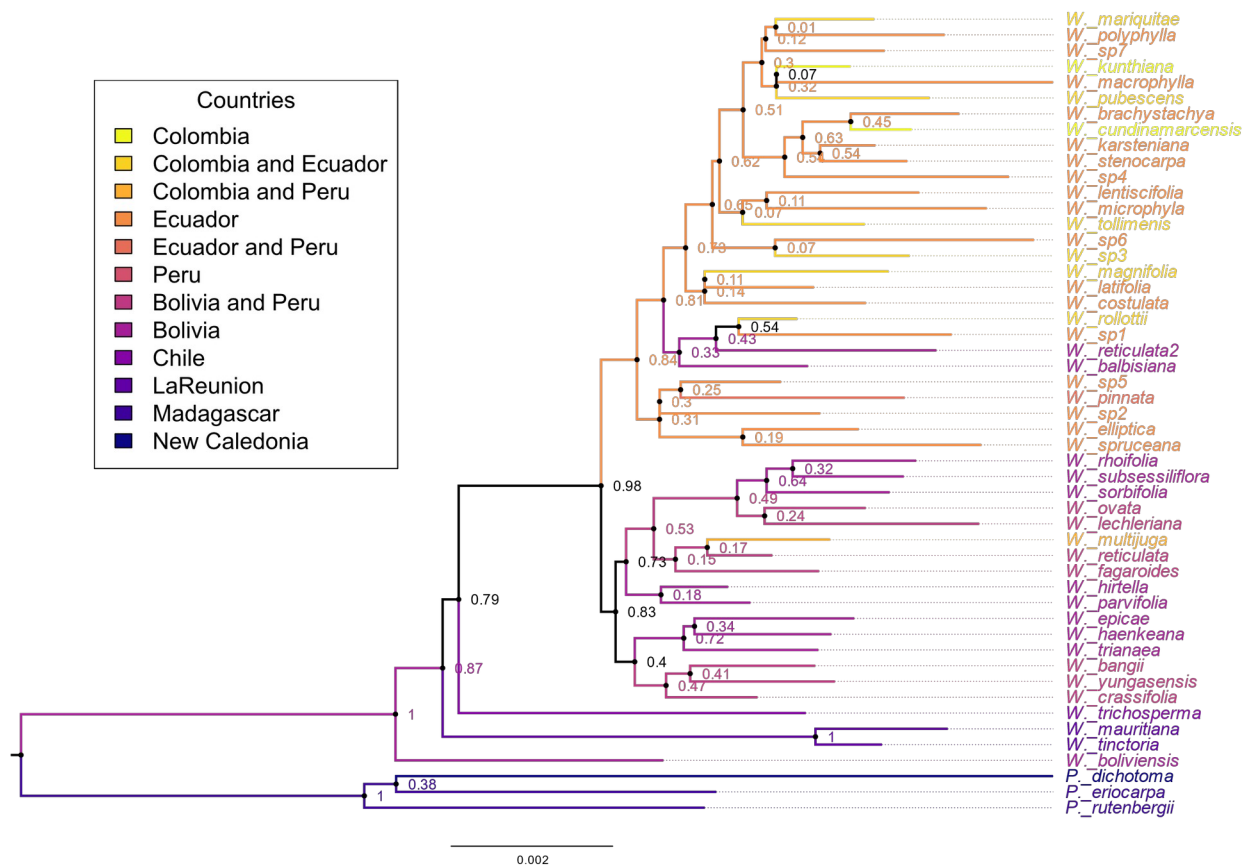


- Countries
- Colombia
  - Ecuador
  - Peru
  - Bolivia
  - Chile
  - LaReunion
  - Madagascar
  - New Caledonia

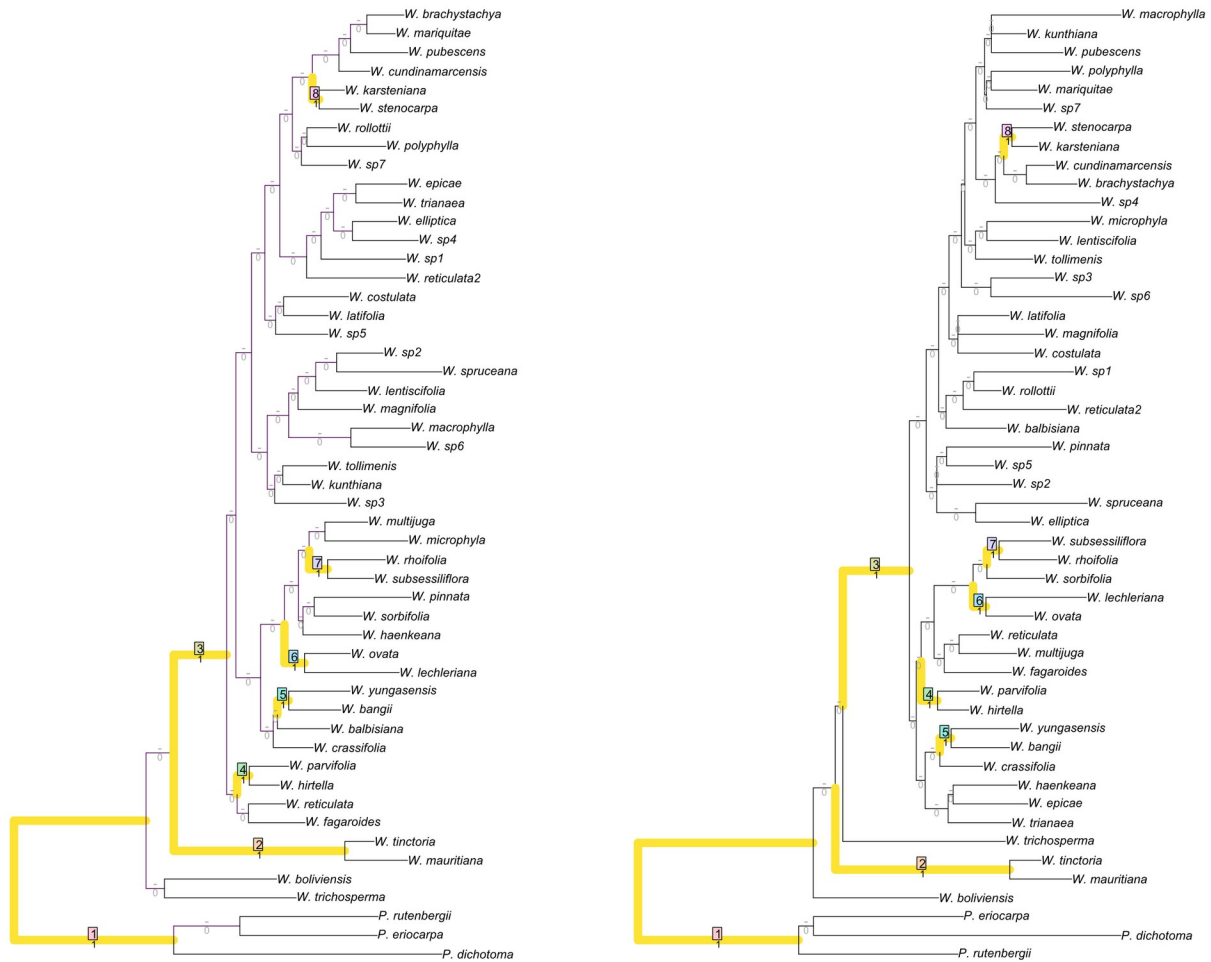
0.002

## Supplementary Figure 2. Species-level Phylogeny for *Weinmannia*.

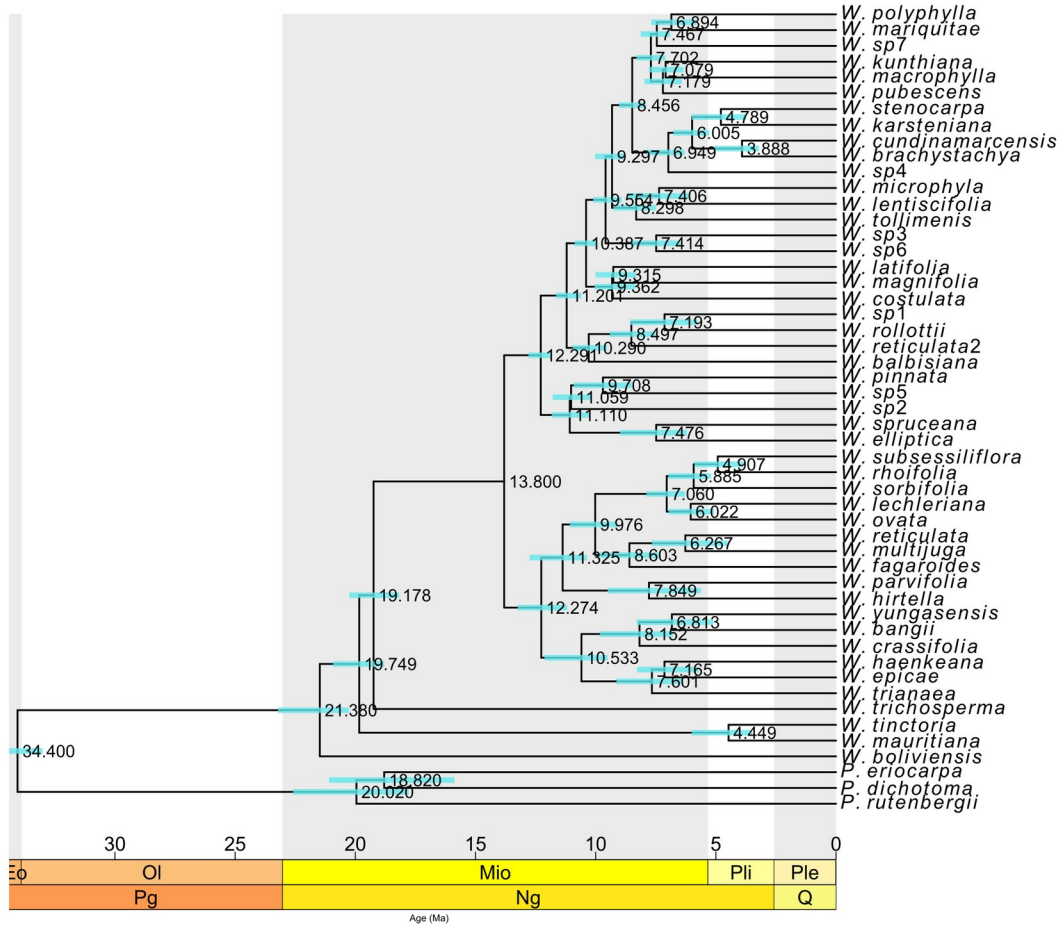
SVDQuartets tree inferred from concatenated 2bRAD-seq data from 48 individuals of *Weinmannia* plus 3 individuals in the outgroup. Bootstrap support values are shown as node labels, tip labels and branches are colored by country where species were collected. Branch labels were estimated using RAxML using this topology, (see methods).



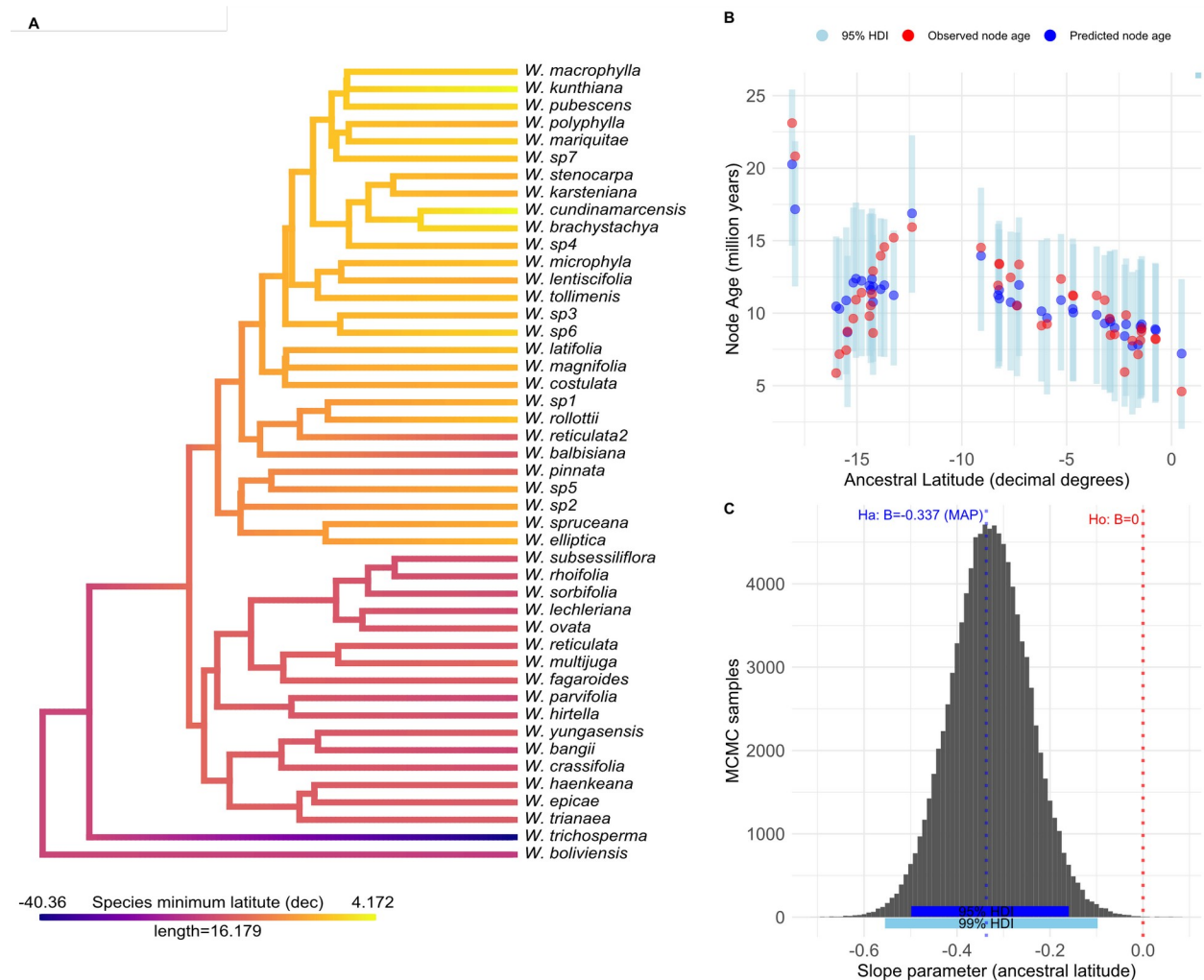
**Supplementary Figure 3. Comparison of RAXML and SVDQuartets Species - level trees.** *Weinmannia* phylogeny for both methods are compared by highlighting in yellow common splitting patterns. The number of ceros depicted at the nodes trees represent Robinson-Foulds distance, among both trees. (Figure generated with TreeDist Package in R)



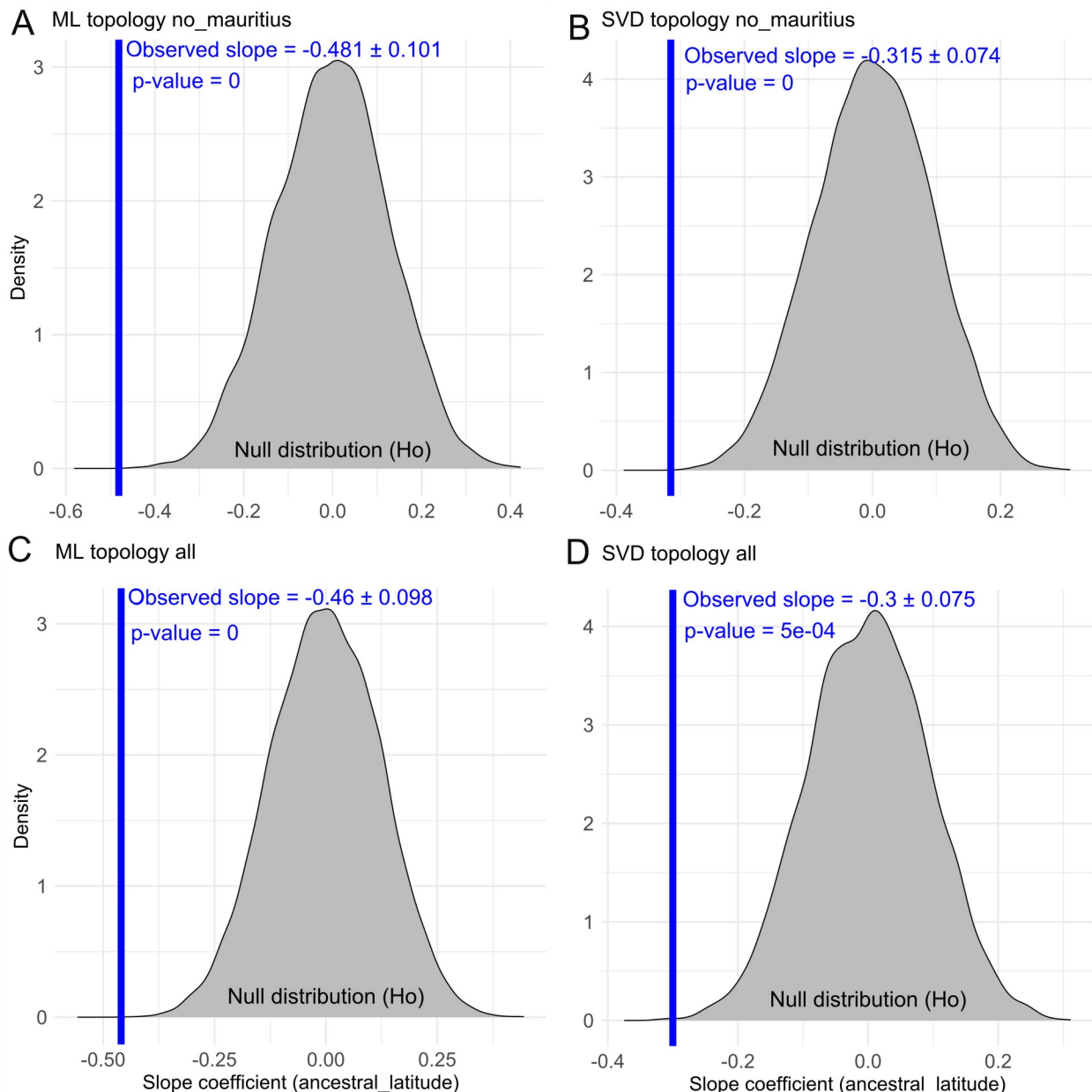
**Supplementary Figure 4.** SVDQuartets phylogeny with estimated divergence times of *Weinmannia* species. Median divergence age estimates across bootstrap trees with 95% confidence intervals in blue bars (see methods).



**Supplementary Figure 5. Analysis for testing the dispersal from southern latitudes towards the North Andes through the Andes using topology inferred with SVDQuartets excluding Mascarene species. A. Ancestral character estimate for latitude of hypothetical ancestors (nodes).** Ancestral states were reconstructed on the SVDQuartets timetree using the minimum latitude of each of the 46 South American *Weinmannia* species considering reviewed accessions. The colors in the figure depict a continuous gradient of latitude, transitioning from southern temperate regions in blue to northern tropical regions in yellow, with intermediate latitudes in the central Andes represented in red. **B. Bayesian linear regression of node age as a function of predicted ancestral latitude: Posterior predictive check.** Observed values are represented in red dots. The blue dots represent the maximum a posteriori estimates, skyblue bars represent 95% High density intervals (HDI). **C. A posteriori probability distribution for the estimated slope coefficient for latitude as a predictor of node age.** Maximum a posteriori (MAP) is equal to  $\beta = -0.337$  and the 95% HDI in blue segment goes from -0.499 to -0.160 which includes zero, and the 99% HDI goes from -0.555 to -0.0975. This result shows the slope is different from zero ( $\beta = 0$ ) rejecting the null hypothesis with a 99% of credibility.



**Supplementary Figure 6. Null-Hypothesis test for the slope coefficient when modelling Node Age as a function of ancestral latitude based on non-parametric bootstrap.** For each topology inferred and subset analysis performed the blue line indicates the estimated slope coefficient for the linear model predicting node age as a function of ancestral latitude. The density plot indicates the null distribution generated with non-parametric bootstrapping. P-value and slope coefficient  $\pm$  standard deviation indicated in label next to blue lines. **A.** Test performed using the Maximum likelihood Species-tree excluding Mascarene species. **B.** Test performed using the SVDQuartet Species-tree excluding Mascarene species. **C.** Test performed using the Maximum likelihood Species-tree including all *Weinmannia* species in this study. **D.** Test performed using the SVDQuartet Species-tree including all *Weinmannia* species in this study.

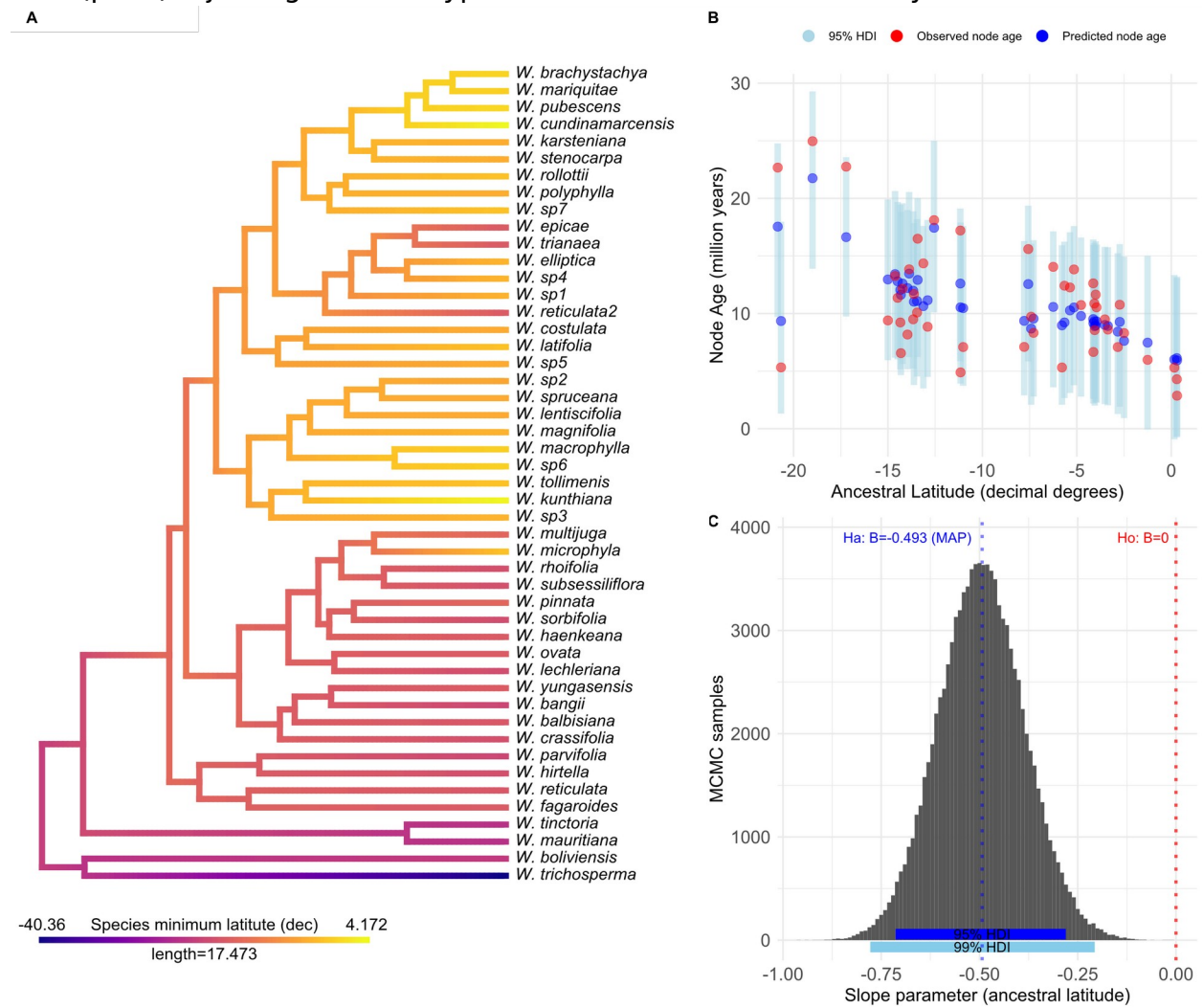


**Supplementary Figure 7. Analysis for testing the dispersal from southern latitudes towards the North Andes through the Andes using topology inferred with Maximum Likelihood including Mascarene species. A. Ancestral character estimate for latitude of hypothetical ancestors (nodes).**

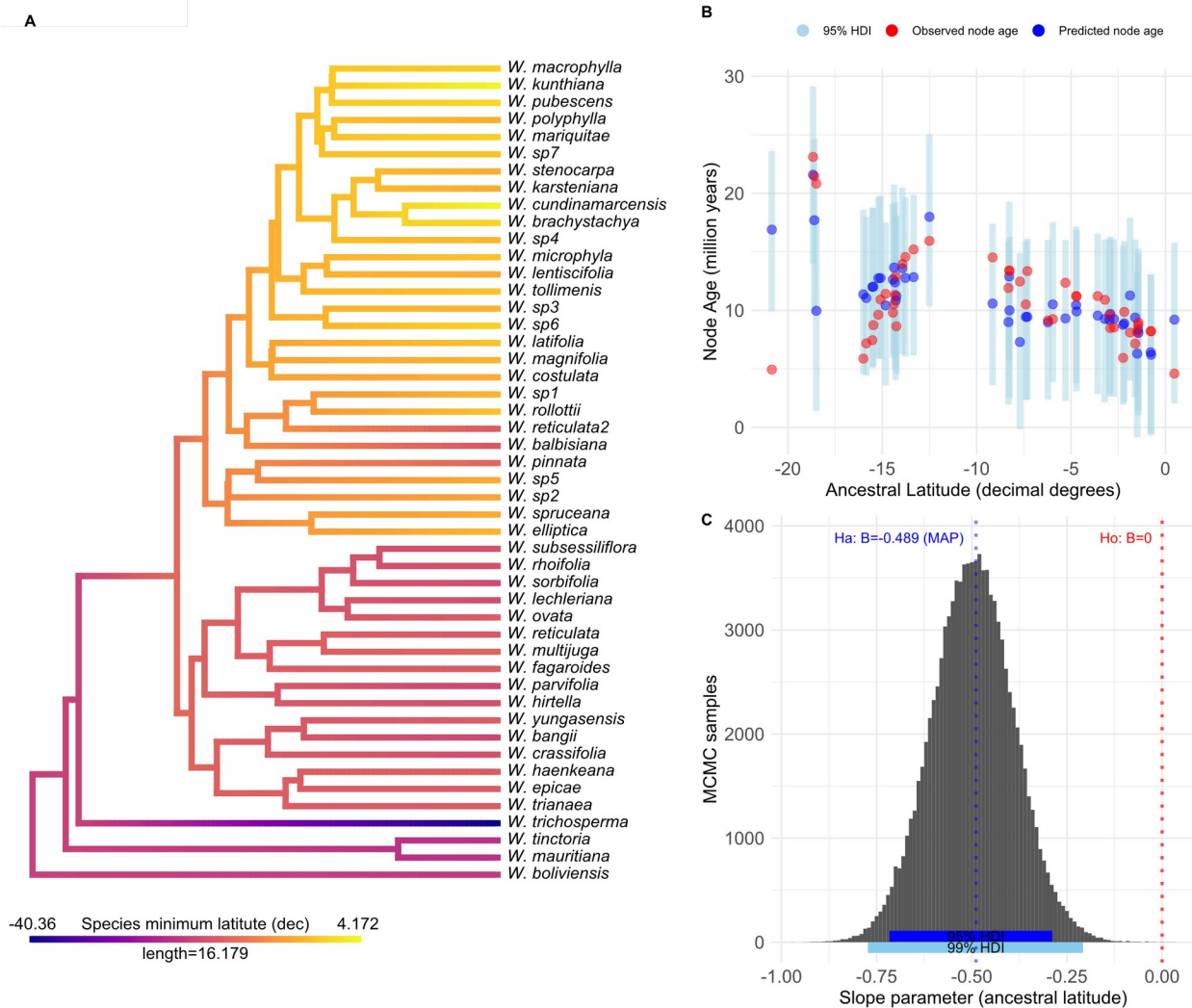
Ancestral states were reconstructed on the SVDQuartets timetree using the minimum latitude of each of the 48 *Weinmannia* species in this study considering reviewed accessions. The colors in the figure depict a continuous gradient of latitude, transitioning from southern temperate regions in blue to northern tropical regions in yellow, with intermediate latitudes in the central Andes represented in red.

**B. Bayesian linear regression of node age as a function of predicted ancestral latitude: Posterior predictive check.** Observed values are represented in red dots. The blue dots represent the maximum a posteriori estimates, skyblue bars represent 95% High density intervals (HDI).

**C. A posteriori probability distribution for the estimated slope coefficient for latitude as a predictor of node age.** Maximum a posteriori (MAP) is equal to  $\beta = -0.493$  and the 95% HDI in blue segment goes from -0.713 to -0.280 which includes zero, and the 99% HDI goes from -0.778 to -0.207. This result shows the slope is different from zero ( $\beta = 0$ ) rejecting the null hypothesis with a 99% of credibility.

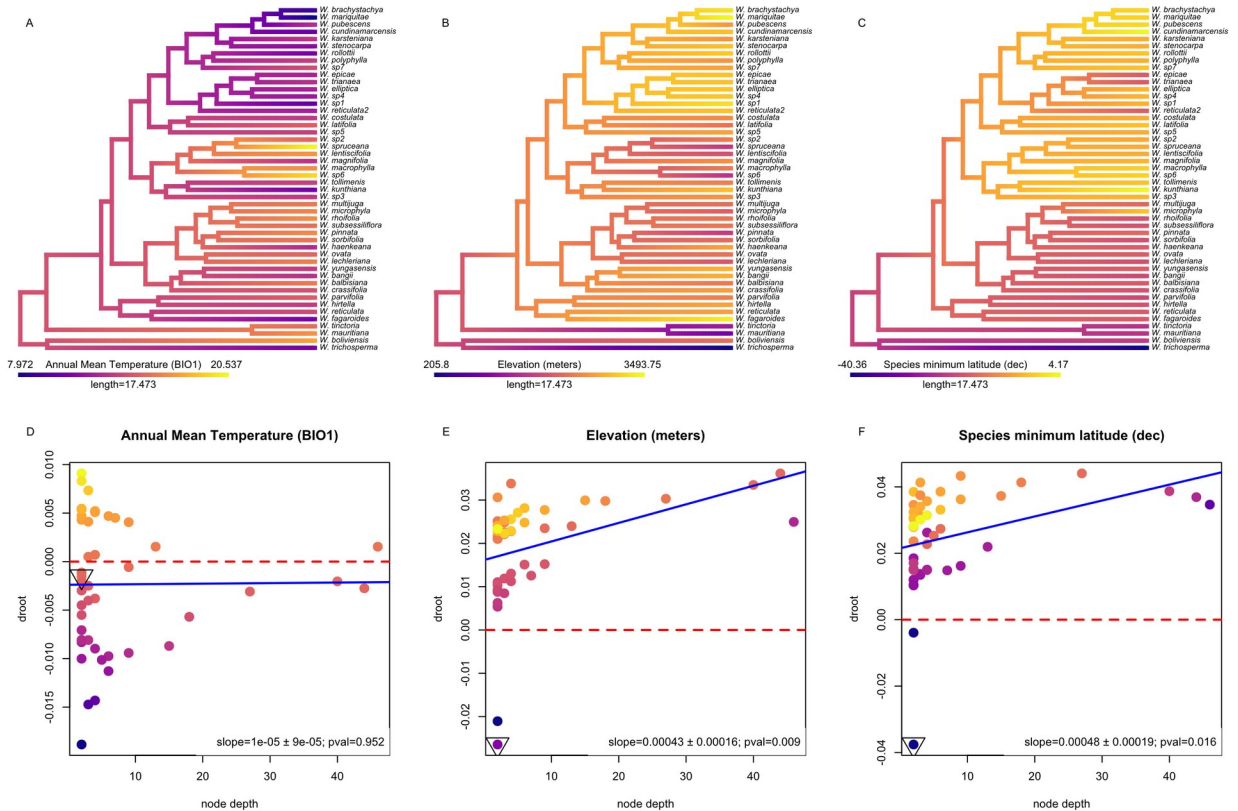


**Supplementary Figure 8. Analysis for testing the dispersal from southern latitudes towards the North Andes through the Andes using topology inferred with SVDQuartets including Mascarene species. A. Ancestral character estimate for latitude of hypothetical ancestors (nodes).** Ancestral states were reconstructed on the SVDQuartets timetree using the minimum latitude of each of the 48 *Weinmannia* species in this study considering reviewed accessions. The colors in the figure depict a continuous gradient of latitude, transitioning from southern temperate regions in blue to northern tropical regions in yellow, with intermediate latitudes in the central Andes represented in red. **B. Bayesian linear regression of node age as a function of predicted ancestral latitude: Posterior predictive check.** Observed values are represented in red dots. The blue dots represent the maximum a posteriori estimates, skyblue bars represent 95% High density intervals (HDI). **C. A posteriori probability distribution for the estimated slope coefficient for latitude as a predictor of node age.** Maximum a posteriori (MAP) is equal to  $\beta = -0.489$  and the 95% HDI in blue segment goes from -0.716 to -0.289 which includes zero, and the 99% HDI goes from -0.773 to -0.208. This result shows the slope is different from zero ( $\beta = 0$ ) rejecting the null hypothesis with a 99% of credibility.





**Supplementary Figure 9. Exploratory analysis of thermal niche conservatism and altitudinal niche evolution in relation to latitudinal migration in *Weinmannia*.** Panels A-C show ancestral character reconstruction under Brownian Motion across 48 *Weinmannia* species. Panels D-F display scatterplots of evolutionary rates (droot) vs. node depth with fitted linear models (blue curve), slope estimates are indicated in the bottomleft of each plot and the MRCA of the trichosperma-boliviensis clade is marked by a triangle. Colors represent continuous gradients for each variable: A and D represent mean annual temperature (BIO1), B and E represent elevation, and C and F represent latitude.



**Supplementary Table 1.** Significance test to evaluate whether estimated mean evolutionary rates (droot) differed from zero under linear model  $droot \sim variable - 1$ . Populational mean *droot* estimates (Intercept coefficients), standard errors and wald-test (t and p.val).

<b><i>variable</i></b>	<b><i>estimated mean</i></b>	<b><i>error</i></b>	<b><i>t</i></b>	<b><i>p.val</i></b>
<i>Mean annual temperature</i>	-0.00235	0.00171	-1.372	0.172
<i>Elevation</i>	0.01933	0.00171	11.304	0.000
<i>Latitude</i>	0.02506	0.00171	14.655	0.000

## Supplementary Methods

**Supplementary methods 1 – Bayesian regression.** Bayesian regression analysis. We developed a hierarchical Bayesian regression to assess correlation structures from nesting patterns between phylogenetic nodes, considering evolutionary relationships in latitude observations. The model, implemented in Stan v. 2.18.2 (Carpenter et al. 2017) via Hamiltonian MCMC, was run in R using the rstan package v. 2.26.23 (Stan Development Team 2023). Full Stan code is provided in Supplementary Materials 1. The linear predictor function is defined as:

$$\mu_n = \alpha_{int} + \beta * X_n + \theta_n \quad (1)$$

Where  $\mu_n$  is the linear predictor for the expected node age  $Y_n$  for each observation at node  $n$ ,  $\alpha_{int}$  is the intercept,  $X_n$  is the estimated ancestral latitude,  $\beta$  is the slope representing the change in  $Y$  for a one-unit change in  $X$ , and  $\theta_n$  is the random effect for each node capturing unexplained variation. Random effects were drawn from a multivariate normal distribution, accounting for correlations from shared evolutionary history according to the following function:

$$\theta_n \sim \text{multinormal}(0_N, \Sigma) \quad (2)$$

Where  $0_N$  is a zero-mean vector of length  $N$  (the number of nodes) and  $\Sigma$  is the phylogenetic covariance matrix. We generated this matrix using the `makeL1` function from the `RRphylo` package in R (Castiglione et al. 2018), which constructs an  $N \times N$  matrix of branch lengths for all root-to-node paths, capturing hierarchical relationships between node pair. Node age  $Y_n$  was modeled as a likelihood function with normally distributed error with mean drawn from  $\mu_n$  as follows:

$$Y_n \sim \text{normal}(\mu_n, \varepsilon_n) \quad (3)$$

Where  $\varepsilon_n$  is the residual standard deviation, capturing unexplained variation in Y after accounting for X and random effects ( $\theta$ ). The model was fitted using four independent MCMC chains, each running 3,000,000 iterations. For efficiency, chains were thinned every 10 iterations, yielding 300,000 samples per chain, with the first 50,000 discarded as burn-in. The max\_treedepth was set to 10 to address divergent transitions during sampling.

**Supplementary methods 2 – Exploratory analysis of thermal niche conservatism.** To support our hypothesis of *Weinmannia*'s south-to-north migration with an extratropical origin, we assessed thermal niche conservatism across the phylogeny. We performed ancestral reconstructions of mean annual temperature (BIO1) and elevation using a time-calibrated ML species-level phylogeny. BIO1 values were extracted from WorldClim 2 (Fick & Hijmans 2017) at a 0.5 arc-second resolution, and elevation was estimated from geo-referenced herbarium specimen data.

To evaluate trait conservatism, we used a color gradient to map observed and reconstructed values onto the species-tree edges using the 'contMap' function in phytools v.2.1, under a Brownian motion model. We assessed whether ancestral values at basal nodes were retained throughout the tree by calculating the Darwin ( $d$ ) rate of trait evolution per unit time (Haldane 1949) for each node using reconstructed values of BIO1, Elevation, and Latitude. The rate of change from each node to the root node (putative extratropical ancestor) was calculated as  $d_{root}$ .

As follows:

$$d_{root} = [\ln(X_i) - \ln(X_{root})] / \Delta \text{time} \quad (4)$$

Where  $X_i$  was the estimated value for each  $i$  node and  $X_{root}$  was the estimated value of that same trait for the root node, the MRCA of all *Weinmannia*.  $\Delta time$  is the distance in million years from the root node to the  $i$  node. To statistically assess if  $d_{root}$  differed significantly between the reconstructed traits (BIO1, Elevation, and Latitude), we employed a generalized linear model (GLM) framework fitting a Gaussian GLM without an intercept, allowing the mean  $d_{root}$  to be estimated independently for each trait as follows:

$$d_{root} \sim trait - 1 \quad (5)$$

The resulting coefficients represent the mean  $d_{root}$  for each group (BIO1, Elevation, and Latitude). We used Wald tests from the GLM summary to determine if the mean  $d_{root}$  for each group was significantly different from zero. Estimated values close to zero were taken as evidence for conservatism of the ancestral values across nodes. Additionally, we performed pairwise t-tests to compare the means of  $d_{root}$  between each trait group.

### References Supplementary methods

- Carpenter B., Gelman A., Hoffman M.D., Lee D., Goodrich B., Betancourt M., Brubaker M., Guo J., Li P., Riddell A. 2017. Stan: A Probabilistic Programming Language. *J. Stat. Soft.* 76:1–32.
- Castiglione S., Tesone G., Piccolo M., Melchionna M., Mondanaro A., Serio C., Di Febbraro M., Raia P. 2018. A new method for testing evolutionary rate variation and shifts in phenotypic evolution. *Methods in Ecology and Evolution* 9:974–983.
- Haldane, J.B.S., 1949. Suggestions as to Quantitative Measurement of Rates of Evolution. *Evolution* 3, 51–56.

Stan Development Team. 2023. RStan: the R interface to Stan. R package version 2.26.23.

<https://mc-stan.org/>.